# EFF-1 promotes muscle fusion, paralysis and retargets infection by AFF-1-coated viruses in *C. elegans*

Anna Meledin[1], Xiaohui Li[1], Elena Matveev[1], Boaz Gildor[1], Ofer Katzir[1] and Benjamin Podbilewicz[1]*

[1]Department of Biology, Technion- Israel Institute of Technology, Haifa, 32000, Israel

*Correspondence to: podbilew@technion.ac.il

Running title: Abnormally fused muscles infected by fusexin-coated virus

16 **Graphical abstract:**

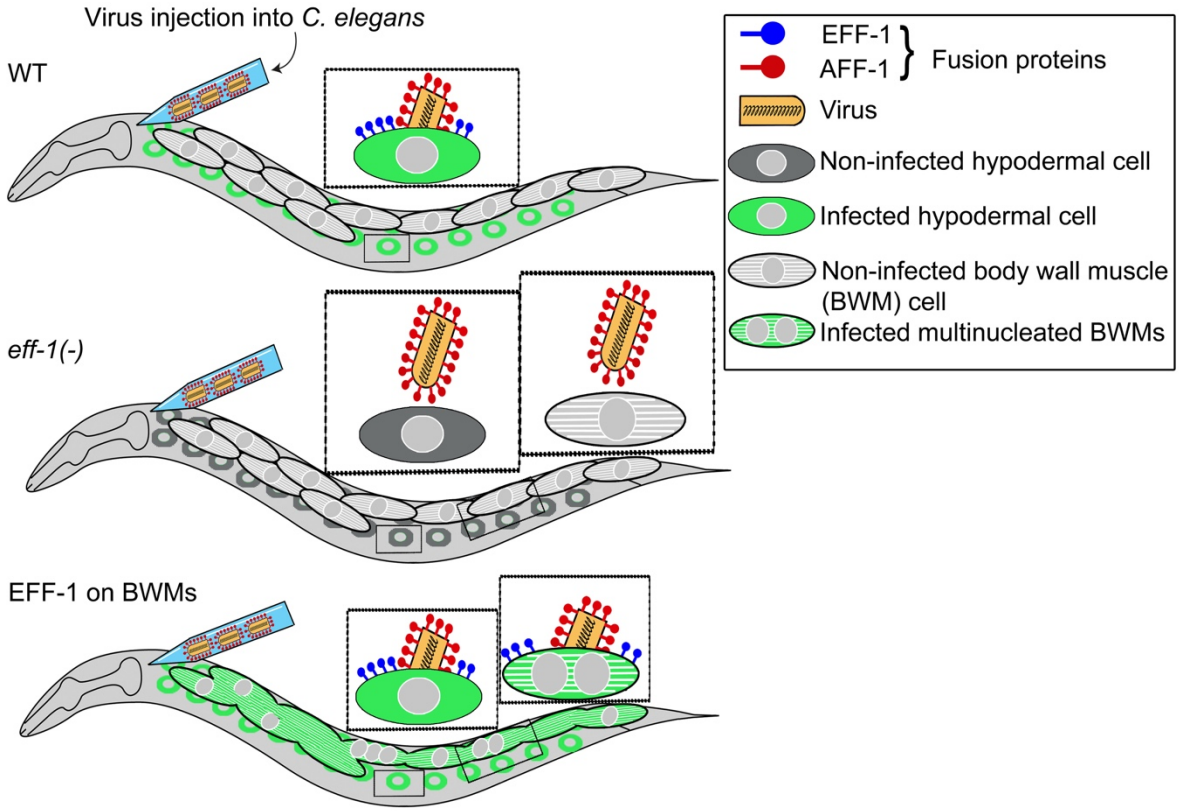


17

18

19 **A hallmark of muscle development is that myoblasts fuse to form myofibers. However,**
20 **smooth muscles and cardiomyocytes do not generally fuse. In *C. elegans*, the body wall**
21 **muscles (BWMs), the physiological equivalents of skeletal muscles, are mononuclear.**
22 **Here, to determine what would be the consequences of fusing BWMs, we express the**
23 **cell-cell fusogen EFF-1 in these cells. We find that EFF-1 induces paralysis and dumpy**
24 **phenotypes. To determine whether EFF-1-induced muscle fusion results in these**
25 **pathologies we injected viruses pseudotyped with AFF-1, a paralog of EFF-1, into the**
26 **pseudocoelom of *C. elegans*. When these engineered viruses encounter cells**
27 **expressing EFF-1 or AFF-1 they are able to infect them as revealed by GFP expression**
28 **from the viral genome. We find that AFF-1 viruses can fuse to EFF-1-expressing**
29 **muscles revealing multinucleated fibers that cause paralysis and abnormal muscle**
30 **morphogenesis. Thus, aberrant fusion of otherwise non-syncytial muscle cells may**
31 **lead to pathological conditions.**

32

## Significance statement

Most cells are individual units that do not mix their cytoplasms. However, some cells fuse to become multinucleated in placenta, bones and muscles. In most animals, muscles are formed by myofibers that originate by cell-cell fusion. In contrast, in *C. elegans* the body wall muscles are mononucleated cells that mediate worm-like movement. EFF-1 and AFF-1 fusogens mediate physiological cell fusion in *C. elegans*. By ectopically expressing EFF-1 in body wall muscles we induce their fusion resulting in behavioral and morphological deleterious effects, revealing possible causes of congenital myopathies in humans. Using AFF-1-coated pseudoviruses we infect EFF-1-expressing muscle cells retargeting viral infection into these cells. We suggest that virus retargeting can be utilized to study myogenesis, neuronal regeneration, gamete fusion and screens for new fusogens in different organisms. In addition, our virus retargeting system can be used in gene-therapy, viral-based oncolysis and to study viral-host interactions.

## Introduction

Vesicular Stomatitis Virus (VSV) is an enveloped negative strand RNA rhabdovirus. VSV utilizes its surface glycoprotein G (VSV-G) to infect vertebrates and invertebrates and lyses many cell lines tested to date [1–3]. VSV is widely used for pseudotyping other viruses and has a high transduction efficiency [1–4]. These properties turned VSVΔG into a promising vector for gene therapy, tissue regeneration, viral-based oncolysis, and VSV-based vaccines, some of which successfully completed phase III clinical trials [1,5]. Moreover, VSV-based vectors are useful for studying mechanisms of transcription and replication of RNA viruses, cellular trafficking, antiviral responses and fusion proteins (fusogens) [6–9]. However, the major bottleneck for both applied and fundamental research purposes is achieving an efficient and specific targeting of VSV-based vectors into desired cells/tissues of a live, multicellular organism [3]. Like other viruses, VSV lacks specificity for desired target cells as it suggestively enters cells through highly ubiquitous receptors such as the LDL receptor [10]. Retargeting VSV into particular tissues of interest therefore requires blocking the virus' natural interactions providing new, cell-specific interactions. Indeed, mutation or substitution of VSV-G with glycoproteins from other viruses or chimeric glycoproteins coupled with antibodies can retarget VSV to specific cells [3,4,11–13].

VSV-G is a class III viral fusogen whereas the *Caenorhabditis elegans* EFF-1 and AFF-1, which fuse somatic cells during development, are structural homologs of class II viral

proteins and gamete HAP2(GCS1) fusogens from the fusexin family [14–22]. EFF-1 and AFF-1 also participate in maintaining neuronal architecture and neuronal reconnection following injury [23–27]. Studied viral glycoproteins, including VSV-G, use a unilateral fusion mechanism that depends on the expression of receptors only on the target cells [28,29]. In contrast, EFF-1 and AFF-1 are bilateral fusogens- their presence is required on the membranes of both apposing cells to mediate fusion [6,16,18,30,31]. These two fusogens can act in either a homotypic or a heterotypic manner [6,16,18,21] and mediate heterotypic cell fusion of Sf9 insect and Baby Hamster Kidney (BHK) cells [6,16]. Finally, VSV viruses containing a *GFP* substituting the *VSV-G* coding sequence (VSV∆G) [32,33] that are coated with AFF-1 (VSV∆G-AFF-1) specifically infect AFF-1 or EFF-1 expressing BHK cells [6]. Thus, in contrast to the pseudotyped virus coated with the native, unilateral G glycoprotein (VSVΔG-G), infection by VSVΔG-AFF-1 requires fusogen expression on the host cell membrane. To date, however, VSVΔG coated with AFF-1, EFF-1 or any other non-viral fusogen have not been tested for infection in a living organism. Recently VSVΔG-G was demonstrated to infect living *C. elegans* [7,34]. Given that: (i) VSVΔG-AFF-1 requires a fusogen on the target cell for infection, (ii) a detailed cellular atlas of AFF-1 and EFF-1 expression and function in *C. elegans* is known and (iii) *C. elegans eff-1* and *aff-1* mutants are available, we test whether VSVΔG-AFF-1 can be retargeted to specific cells in living *C. elegans*. We found that AFF-1-coated viruses infect *C. elegans* and specifically target cells that express functional EFF-1 or AFF-1. Furthermore, AFF-1-coated pseudoviruses can be redirected to mononucleated body wall muscles (BWMs) that ectopically express EFF-1. Thus, the new delivery system enabled us to observe that EFF-1-induced BWMs merger and formation of non-functional syncytial muscle fibers, demonstrating the consequences of aberrant muscle fusion in an animal that normally uses mononucleated muscles for gait. Based on our results, we propose that in *C. elegans* a layer of longitudinal mononucleated muscles electrically coupled by gap junctions efficiently mediate wavelike movement and ectopic fusion disrupts the morphology and physiology of the muscular system. We also suggest additional applications for VSVΔG-AFF-1 including finding new fusogens and fusogen-expressing tissues, studying fusogen-fusogen interactions and fusogen-interacting proteins *in vivo,* studying neuronal regeneration processes and using specific cell-delivery approaches for other viruses such as coronaviruses and retroviruses in *C. elegans* and in other organisms.

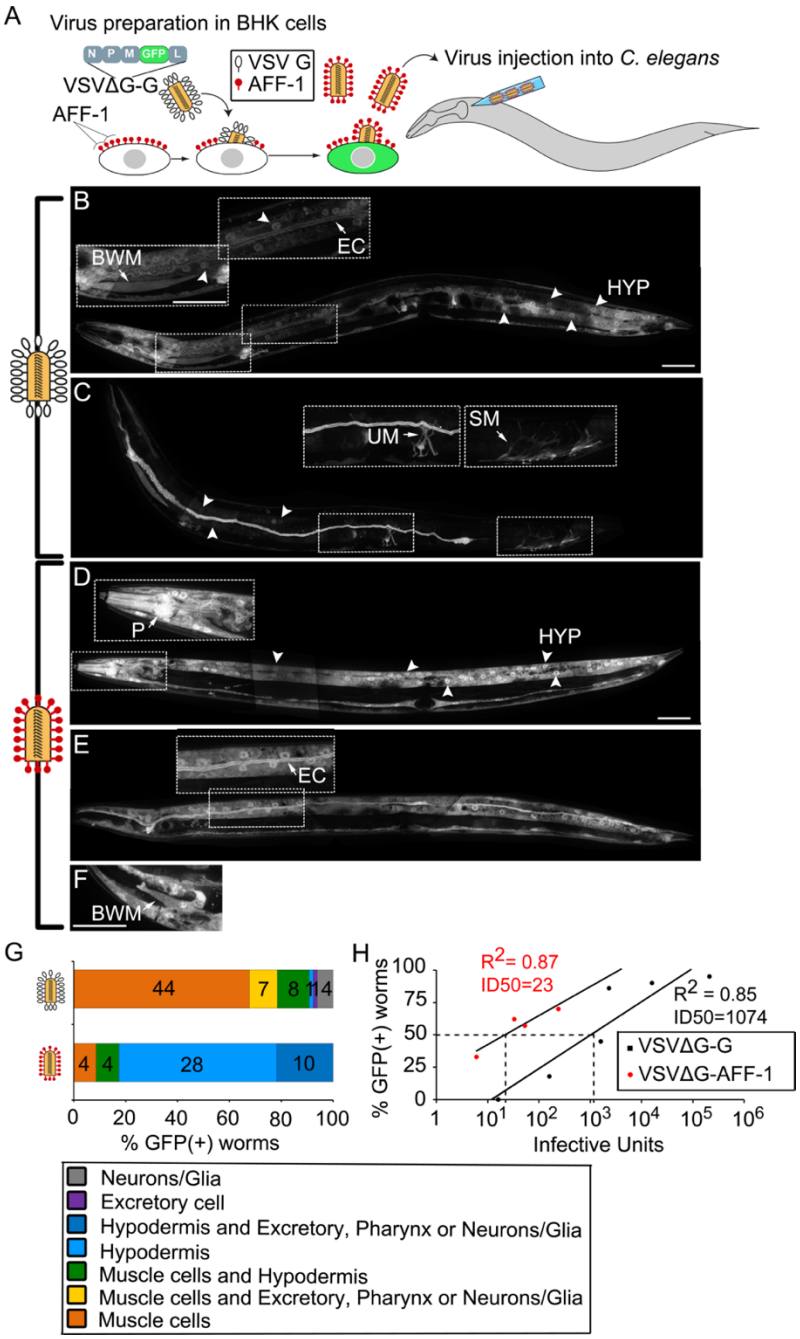


**Figure 1. VSVΔG-AFF-1 and VSVΔG-G have different tropisms**

**(A)** BHK cells expressing AFF-1 (red pins) were infected with VSVΔG-G. The viral genome encodes GFP replacing VSV-G (white pins). GFP(+) (green), infected cells. VSVΔG-AFF-1 pseudoviruses were harvested from the supernatant, titrated and microinjected into *C. elegans*. **(B-F)** Confocal Z-stack projections of *drh-1* worms injected with VSVΔG-G (2300-16000 IU) or VSVΔG-AFF-1 (33-240 IU) and imaged 48-72 h later (VSVΔG-G, n=65; VSVΔG-AFF-1, n=46 from 5 and 6 independent experiments respectively). Images and their insets are dot boxed. Arrowheads, hypodermal (HYP) nuclei. Arrows, infected cell. BWM-Body Wall Muscle, UM-Uterine Muscle, SM-Stomatointestinal Muscle, EC-Excretory Cell, P-Pharynx. Scale bars, 50 µm. **(G)** Distribution of worms with specified infected, GFP(+) cell types. **(H)** Fraction of GFP(+) worms injected with indicated IU of VSVΔG-G or VSVΔG-AFF-1. Each dot represents an independent experiment (n=10-28 worms per experiment). $R^2$ and the IU doses producing 50% GFP(+) worms (ID50) are indicated. See also Figure S1.

## Results

### VSV∆G-AFF-1 and VSV∆G-G infect mostly hypodermal and muscle cells respectively

Wildtype, recombinant or pseudotyped VSV has been shown to infect rodents, fish, farm animals, and primates [1,35–37]. Recently, VSVΔG-G was shown to infect *C. elegans* [7]. Previously, pseudotyped VSV expressing the *C. elegans* somatic fusogen AFF-1 (VSV∆G-AFF-1) was shown to infect AFF-1 or EFF-1 expressing BHK cells [6], but was not tested in a living organism. To test whether pseudotyped VSV∆G-AFF-1 [6,33,38] can infect *C. elegans*, we prepared a recombinant VSV strain encoding the fluorescent reporter GFP, coated by AFF-1 fusion protein (VSV∆G-AFF-1). Briefly, BHK cells expressing AFF-1 were infected with VSV∆G-G helper virus (Fig. 1A). Newly generated virions were coated by plasma membrane-bound AFF-1, thereby producing VSV∆G-AFF-1 pseudotyped viruses. Then, we titered the viruses determining the number of viral Infective Units (IU)/ml in BHK-AFF-1 cells. Finally, VSV∆G-AFF-1 viruses were injected into worm's pseudocoelom; a body cavity filled with fluid that surrounds the internal organs. We expected that virus injected into the pseudocoelom will encounter different cells inside the worm (Figure 1A). Worms were injected with VSV∆G-AFF-1 that was pre-incubated with αVSV-G antibody (see materials and methods and Figure S4), VSV∆G-G (as a positive control) or DMEM medium (as negative control). We used *drh-1(-)* (Dicer Related Helicase -1) mutant worms, as they are more susceptible to VSV infection and do not have any observable phenotypes [7,34]. Taken that VSV-G works unilaterally, while AFF-1 and EFF-1 fusogens have to be present in both fusing membranes [6,16,18,30], we hypothesized that VSV∆G-G and VSV∆G-AFF-1 will produce different infection patterns. Hence, we characterized and compared the GFP positive (GFP(+)) cells infected by VSV∆G-G or VSV∆G-AFF-1. VSV∆G-G preferentially infected muscle cells, including BWM [7], uterine muscles (UM) and stomatointestinal muscles (SM, Figures 1B and 1C). VSV∆G-G also infected the epidermal cells (hypodermis, HYP), excretory canal cell (EC, Figure 1B), glia and neurons in the head (Figures S1A-S1C). In contrast, VSV∆G-AFF-1 infected mostly HYP cells (Figure 1D), and also excretory cell (Figure 1E) pharyngeal muscles (P) (Figure 1D), BWM (Figure 1F) and head neurons and glia (Figures S1D-S1F). VSV∆G-G infects muscles that do not express any known fusogen (67% of infected, GFP(+) worms had only BWM infection), whereas VSV∆G-AFF-1 mainly infects the EFF-1-expressing hypodermis (61% of GFP(+) worms had only hyp infection) (Figure 1G). Moreover, the calculated ID50 (infection dose producing 50% GFP(+) worms) for VSV∆G-G and VSV∆G-AFF-1 were approximately 1000 and 20 IU respectively (Figure 1H). Therefore, VSV∆G-AFF-1, a virus pseudotyped with a bilateral fusogen, can efficiently infect a multicellular organism such as *C. elegans*. Moreover, VSV∆G-AFF-1 and VSV∆G-G are specialized for different cellular targets and have different infectivity levels.

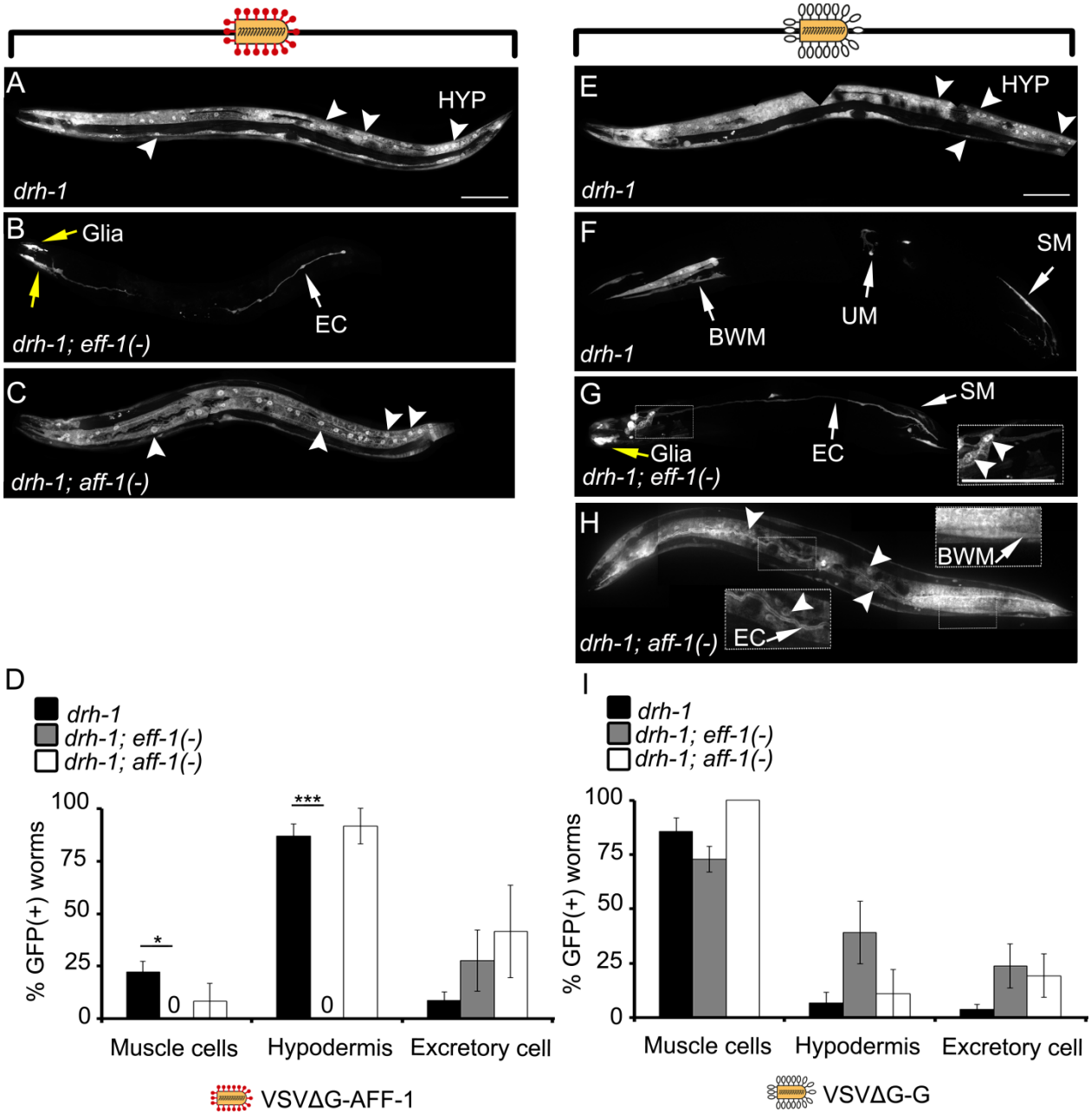


**Figure 2. VSVΔG-AFF-1 requires EFF-1 on target cells for infection**
**(A-C)** Confocal Z-stack projections of *C. elegans* infected with VSVΔG-AFF-1 (33-240 IU) and imaged 48 h later. *drh-1* (n=46), *drh-1;eff-1(-)* (n=15) and *drh-1;aff-1(-)* (n=10).
**(D)** Fraction of GFP(+) worms from (A-C).
**(E-H)** Confocal Z-stack projections of *C. elegans* infected with VSVΔG-G (2300-4700 IU) 48 h post-injection. *drh-1* (n=56), *drh-1;eff-1(-)* (n=39) or *drh-1;aff-1(-)* (n=15).
**(I)** Fraction of GFP(+) worms from (E-H).
Arrowheads, HYP nuclei. Arrows, infected cell. See Figure 1 for cell types. Scale bars, 100 µm. Error bars represent mean ± SEM. *p<0.05, ***p<0.001 (Student's t- test).
See also Figure S2.

163 **VSV∆G-AFF-1 requires EFF-1 in host cells for infection**

164 We showed that cells infected by VSV∆G-AFF-1 included hypodermis, excretory cell, neurons
165 in the head, glia and pharyngeal cells. It is known that in adults pharyngeal cells, head
166 neurons, glia and hypodermal cells express EFF-1 [14], while pharyngeal cells, excretory duct
167 cell and glia express AFF-1 [18,21] and lastly, excretory cell, head neurons, hypodermal cells
168 and pharyngeal cells express EFF-2, a recent duplication of EFF-1 with unknown function
169 (BG, Oren-Suissa and BP unpublished data). Importantly, BWM cells that do not express any
170 known fusogen in *C. elegans* were infected by VSV∆G-AFF-1 in only 9% of the worms
171 compared to 67% of the worms infected with VSV∆G-G (Figure 1G). These findings suggest
172 that infection of living *C. elegans* by VSV∆G-AFF-1 follows a bilateral action mechanism, and
173 that VSV∆G-AFF-1 is capable of interacting with several members of the fusexin family on the
174 target cell. Therefore, we hypothesized that EFF-1-expressing hypodermal cells could not be
175 infected by VSV∆G-AFF-1 in the absence of EFF-1, while cells expressing AFF-1 or EFF-2
176 would still be targeted. To test this hypothesis, we injected either VSV∆G-G or VSV∆G-AFF-
177 1 into the pseudocoelom of wt, null *eff-1(ok1021)* mutants *((eff-1(-);*[14]), null *aff-1(tm2214)*
178 mutants ((*aff-1(-)*;[18]) or putative null *eff-2(hy51)* (*eff-2(-)*; see materials and methods) worms,
179 and quantified the percentage of worms with GFP(+) cells. We detected VSV∆G-AFF-1
180 infected hypodermal cells in *eff-1(+)* (Figure 2A) but not in in *eff-1(-)* worms (Figure 2B), while
181 GFP(+) excretory and glia cell were detected even in the absence of EFF-1 (Figure 2B). *aff-*
182 *1(-)* worms had GFP(+) hypodermal cells as in wildtype (Figure 2C). Overall, the fraction of
183 worms showing VSV∆G-AFF-1-infected hypodermal cells was similarly high in wildtype and in
184 *aff-1(-)* (87% and 92% for wt and *aff-1(-),* respectively) but was absent in *eff-1(-)* mutants
185 (Figure 2D). In addition, muscles were inefficiently infected in wildtype and *aff-1(-)* mutants,
186 and not infected in *eff-1(-)* animals (Figure 2D). The fraction of worms with GFP(+) excretory
187 cells was not significantly different in all backgrounds (Figure 2D). Finally, the fraction of
188 worms with GFP(+) glia/neuron cells was significantly higher in *eff-1(-)*, compared to wt and
189 *aff-1(-)* animals (Figures S1D-S1F). Moreover, *eff-2(-)* and wildtype animals were similarly
190 infected in their hypodermal, muscle and excretory cells (Figure S2). These results show that
191 VSV∆G-AFF-1 requires EFF-1 expressed on hypodermal cells, for their infection. Moreover,
192 we show evidence for AFF-1-EFF-1 bilateral heterotypic interactions *in vivo*.

193 EFF-1 mediates formation of hyp7 syncytium by fusing 139 hypodermal cells during
194 embryonic and larval development and *eff-1(-)* worms have mononucleated hypodermal cells
195 instead of this syncytium [14]. To exclude the possibility that hypodermal cells of *eff-1(-)* worms
196 have a reduced susceptibility to viral infection, we injected wt, *aff-1(-)* and *eff-1(-)* worms with
197 VSV∆G-G. We found that wild-type worms injected with VSV∆G-G, presented a full body-
198 length covered by infected hypodermal cells along with muscles and excretory cells (Figures

199 2E-2F), while *eff-1(-)* worms had only few GFP(+) hyp nuclei localized closer to the injection
200 region- the head, as well as muscles and excretory cells (Figure 2G). *aff-1(-)* worms had
201 hypodermal infection similar to wt animals (Figure 2H). Yet, the fraction of worms injected with
202 VSV∆G-G that showed GFP(+) muscle and hypodermal cells was not significantly different in
203 wt, *eff-1(-)* and *aff-1(-)* backgrounds (Figure 2I). Finally, we observed a small fraction of worms
204 with GFP(+) glia/neurons in the head with no significant difference between all tested
205 backgrounds (Figures S1A-S1C). Thus, hypodermal cells are not compromised for VSV∆G-G
206 infection even in the absence of EFF-1. In addition, VSV∆G-G with its unilateral viral fusogen
207 infects different cells including muscles, hypodermis, excretory cell, and glia/neurons in an
208 EFF-1- and AFF-1-independent manner. This is in contrast to VSV∆G-AFF-1 that uses a
209 bilateral mechanism and infects cells that normally express EFF-1 or AFF-1 in adult animals.
210
211 **VSV∆G-AFF-1-mediated infection depends on *eff-1* activity in target cells**
212 We have shown VSV∆G-AFF-1 fails to infect hypodermal cells in *eff-1(-)* animals (Figure 2).
213 To study whether conditional induction of *eff-1* can trigger infection by VSV∆G-AFF-1 we
214 varied the dosage of *eff-1* using temperature shifts in a conditional temperature sensitive (ts)
215 mutant [14,25]. In *eff-1(hy21ts)* animals grown at the permissive 15°C, most epidermal cells
216 fuse to form multinucleated hypodermis and vulva [14]. However, when *eff-1(hy21)* animals
217 are grown at the restrictive 25°C, epidermal cells fail to fuse, producing phenotypes similar to
218 the null *eff-1(ok1021)* worms [16]. Therefore, *eff-1(ts)* worms can serve as a temperature
219 inducible system for modification of EFF-1 dosage *in vivo* [14,19,25]. To obtain varying
220 expression of EFF-1, we maintained *eff-1(ts)* animals at 15°C, 25°C or performed 25°C to
221 15°C downshifts at different developmental stages and then injected VSV∆G-AFF-1 into
222 young adult worms (Figure 3A). Wildtype worms in all experimental conditions had GFP(+)
223 hyp nuclei spanning the worm's body from head to tail (Figures 3B-3E), while *eff-1(ts)* animals
224 maintained at the restrictive temperature and then shifted down from 25°C to 15°C, had a
225 gradual increase in infected GFP(+) hyp cells (Figures 3F-3I). In wt worms maintained in all
226 conditions, the number of GFP(+) hypodermal nuclei was about 69, consistent with the number
227 of hyp7 nuclei found on one side of the animals body [39,40]. In contrast, for *eff-1(ts)*, the
228 longer time the worms developed at the permissive temperature (15°C), the more GFP(+) hyp
229 nuclei were scored (Figure 3J). Thus, hypodermal infection by VSV∆G-AFF-1 increases with
230 conditional induction of *eff-1*.
231

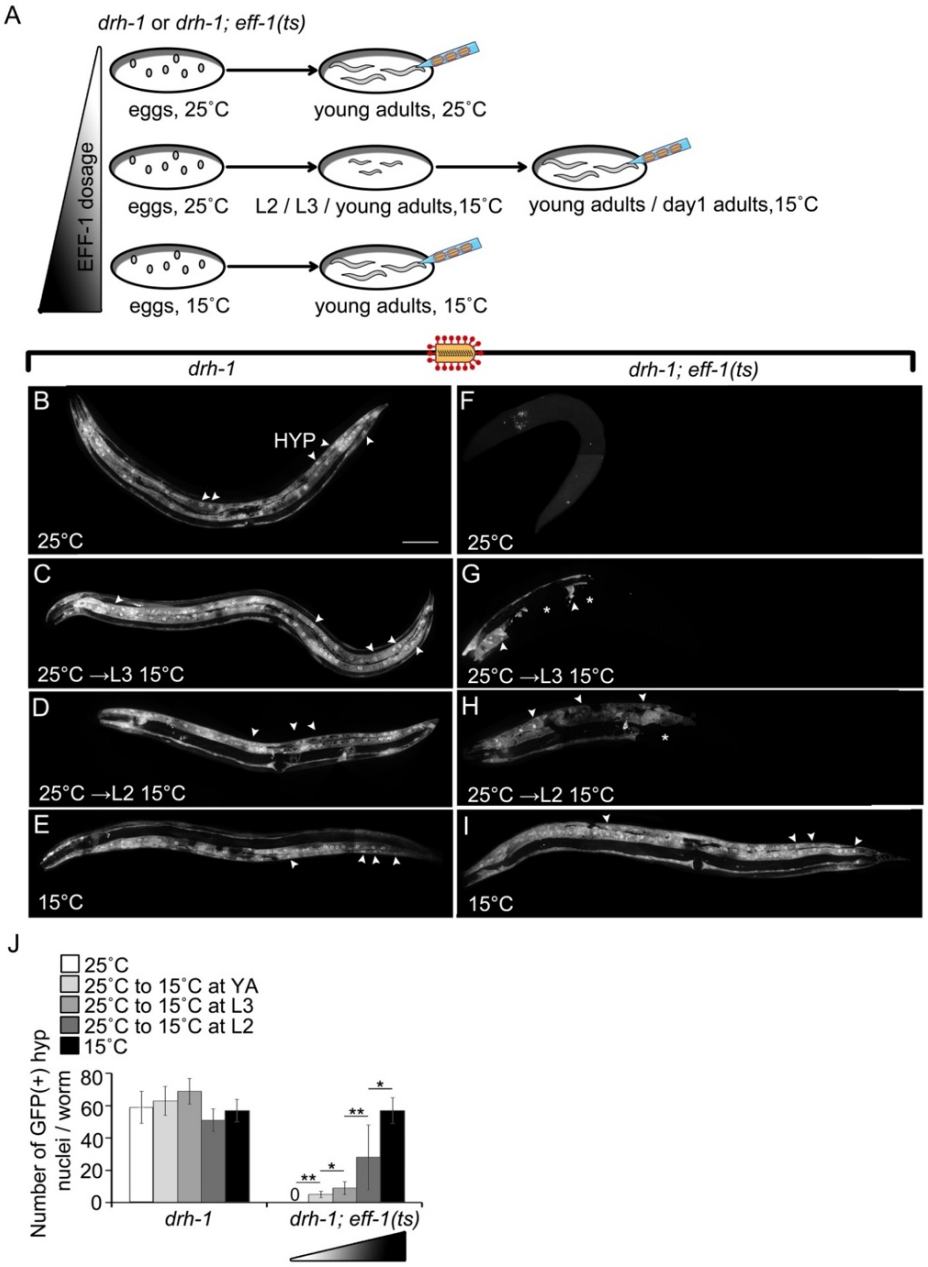


**Figure 3. Infection by VSVΔG-AFF-1 increases with induction of EFF-1 function**

**(A)** Wt or temperature sensitive *eff-1(ts)* animals were maintained at permissive (15°C) or restrictive (25°C) temperatures for different times during their development. Each row represents a different experimental condition. Blue needles indicate virus injection. L2, Larval stage 2; L3, Larval stage 3.

**(B-I)** Confocal Z-stack projections of worms infected with VSVΔG-AFF-1. *drh-1* or *drh-1;eff-1(ts*) animals were injected with VSVΔG-AFF-1 (7-125 IU) as adults, and imaged 48 h later. Arrowheads, HYP nuclei. Asterisks, patches of GFP(-) surrounded by GFP(+) hypodermal cells. Scale bar, 100 µm.

**(J)** Quantitation of experiments. Error bars average ± SEM. Student t-test. *p<0.05, **p<0.001. n=3-10 worms per condition. Triangle, dosage of *eff-1*.

245

246 **Ectopic EFF-1 expression in BWMs produces dumpy and uncoordinated worms**

247 We demonstrated that VSV∆G-AFF-1 specifically infects EFF-1 expressing cells and rarely
248 infects muscle cells. In addition, EFF-1-dependent infection could be induced by EFF-1(ts)
249 conditional expression in target cells (Figure 3). Hence, we propose that ectopic EFF-1
250 expression in host cells, such as body wall muscles (BWMs), could retarget VSV∆G-AFF-1
251 into these cells. *C. elegans* has 95 mononucleated rhomboid BWMs, arranged as staggered
252 pairs and bundled in four quadrants that run along the worm's body [41–43]. While most
253 vertebrates and invertebrates have syncytial striated muscles composed of long
254 multinucleated myofibers, in *C. elegans* and other nematodes the BWMs have not been
255 described to fuse and do not form multinucleated myofibers
256 (https://www.wormatlas.org/hermaphrodite/muscleintro/MusIntroframeset.html). Therefore,
257 we hypothesized that EFF-1 expression in BWMs can induce their ectopic fusion, alter their
258 structure, produce muscle-related phenotypes and increase VSV∆G-AFF-1 infection of
259 BWMs. First, we monitored animals with an extra-chromosomal array containing genomic
260 EFF-1 under the muscle-specific *myosin-3* promoter (*myo-3p*::EFF-1), together with *myo-*
261 *3p::*mCherry which labels cytoplasm and nuclei in BWMs, enteric, gonadal and vulval muscles.
262 Most adult animals, including *myo-3p*::mCherry (+) and (-), were wild-type-like (Table S1,
263 Figures 4A-4B and Movie S1), while about 10% of animals were both *myo-3p*::mCherry(+)
264 and had an uncoordinated and dumpy (Unc+Dpy) phenotype (Table S1, Figures 4C-4D and
265 Movie S1). Most *myo-3p*::mCherry(+), Unc+Dpy animals arrested during larval development
266 (Table S1) with additional phenotypes including bridged BWMs behind the terminal bulb (0/12
267 wt-like worms and 9/15 Unc+Dpy worms), mCherry-labeled aggregates that could be
268 observed with DIC (0/12 wt-like worms and 9/15 Unc+Dpy worms) (Figures 4E-4H), *myo-*
269 *3p*::mcCherry(+) BWMs with clustered nuclei (3/12 wt-like worms and 9/15 Unc+Dpy worms)
270 and elevated number of nuclei/ BWM cell (1.4±0.2 and 2.2±0.3 nuclei/BWM cell in wt-like vs
271 Unc+Dpy larvae respectively) (Figures 4E-4I). While ectopic *hsp*::EFF-1 expression causes
272 embryonic lethality [14,19,25], we found no difference between the fractions of *myo-*
273 *3p*::mCherry (+) and (-) unhatched eggs (Table S1). Thus, EFF-1 expression in BWMs
274 accounts for the Unc+Dpy phenotypes, larval arrest and clustered BWM nuclei, which
275 supports the hypothesis that ectopic EFF-1 induces BWMs multinucleation by cell-cell fusion
276 causing behavioral and morphological phenotypes.

277

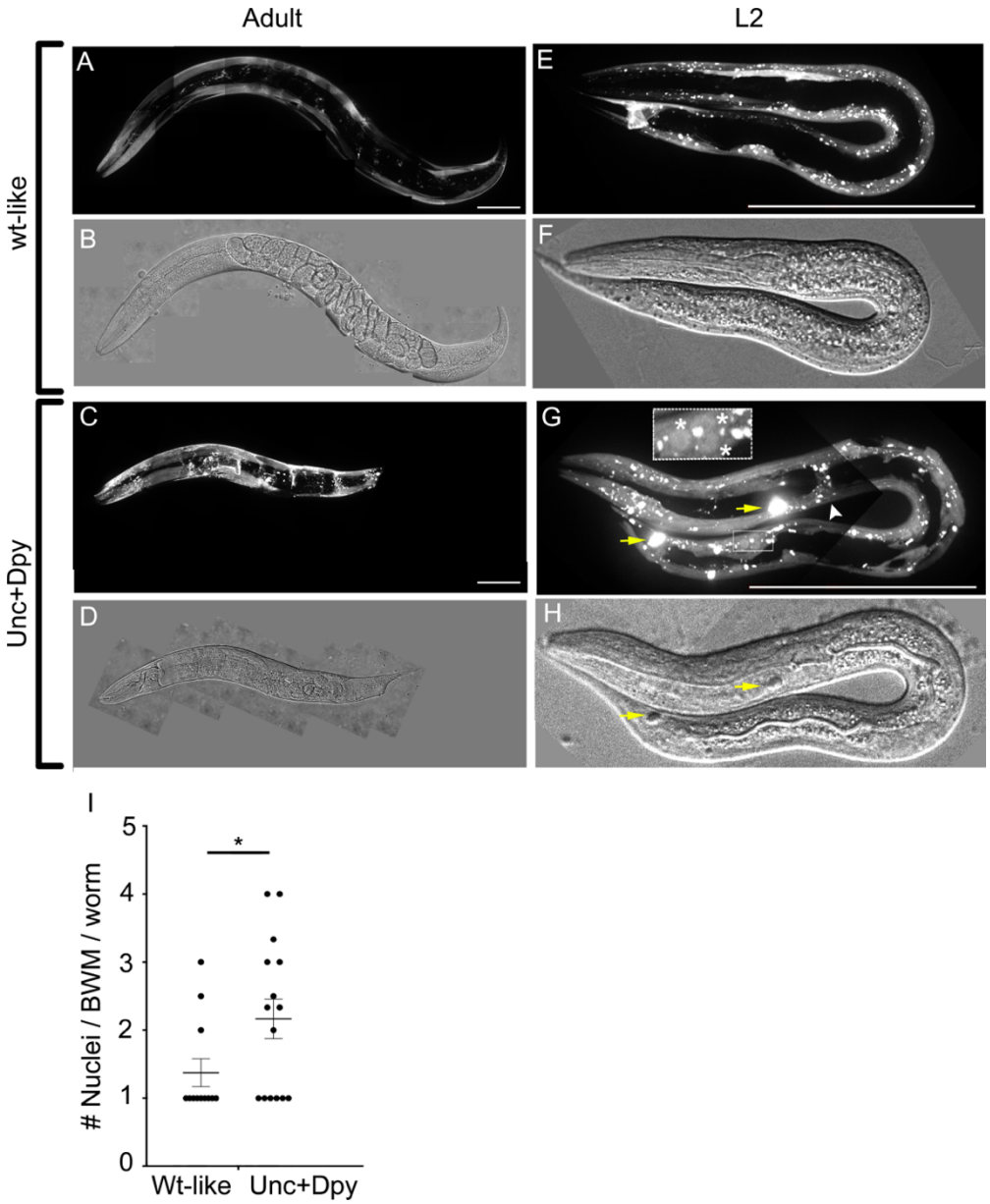


**Figure 4. EFF-1 expression in BWMs produces Unc+Dpy worms with multinucleated cells**

**(A-H)** Images of fluorescent Z-stack projections and respective DIC of animals with extrachromosomal *myo-3p*::EFF-1*, myo-3p*::mCherry. (G) White arrowhead, bridge formed between 2 BWMs from opposing quadrants. Yellow arrows, *myo-3p*::mCherry accumulations also in DIC (H). Asterisks, clustered nuclei within one BWM. Scale bars, 100 µm.

**(I)** Number of nuclei per *myo-3p*::mCherry (+) BWM cell in L2s. wt-like (n=12); Unc+Dpy (n=15). Each dot represents the average number of nuclei/BWM cell/worm. Total average ± SEM for each phenotype. Two tailed Student's t-test $p<0.05$*.

See also Table S1.

**EFF-1 expression in BWMs induces their fusion and retargets VSV∆G-AFF-1 to muscles**

To determine whether EFF-1 expression in BWMs can induce their fusion, we imaged BWMs expressing a membrane-bound YFP (MB::YFP), *myo-3p*::EFF-1 and *myo-3p*::mCherry, (see materials and methods). BWMs of wt-like worms have a normal spindle-shaped morphology

294 with cellular membranes between adjacent BWMs showing different levels of cytoplasmic
295 *myo-3p*::mCherry (as *myo-3p*::mCherry is an extrachromosomal array) (Figures 5A-5C). In
296 contrast, Unc+Dpy worms had disordered muscle fiber structure, the membranes surrounding
297 the BWMs were indistinguishable and the BWMs showed an evenly distributed cytoplasmic
298 *myo-3p*::mCherry indicating fusion and content mixing between these cells during
299 development (Figures 5D-5F). Thus, EFF-1 expression in BWMs induces disappearance of
300 cellular membranes and cytoplasmic merger, suggesting that EFF-1-mediated cell-cell fusion
301 alters BWM structure, likely resulting in Unc+Dpy and larval arrest phenotypes.
302 We showed that VSVΔG-AFF-1 infects EFF-1-expressing hypodermal cells in >80%
303 of the infected worms but infects muscle cells that do not express EFF-1 in about 20% of the
304 infected animals (Figure 2D). Moreover, EFF-1 expression in BWMs induced their fusion, and
305 generated Unc+Dpy worms (Table S1, Movie S1 and Figures 4A-4D and 5A-5F). Taken that
306 EFF-1 and AFF-1 are bilateral fusogens and VSVG is a unilateral fusogen, we hypothesized
307 that ectopic expression of EFF-1 in BWMs would increase their infection by VSVΔG-AFF-1
308 but not by VSVΔG-G. Therefore, we injected either VSVΔG-AFF-1 or VSVΔG-G into the
309 pseudocoelom of worms ectopically expressing EFF-1 and mCherry in BWMs and imaged
310 them. For VSVΔG-AFF-1 but not for VSVΔG-G, the fraction of infected BWMs was significantly
311 higher in Unc+Dpy worms (expressing the *myo-3p*::mCherry marker) compared to wt-like
312 (expressing the *myo-3p*::mCherry marker) and wt animals (Figure 6). Thus, EFF-1 expression
313 in BWMs retargets VSVΔG-AFF-1 into muscles but does not affect the natural VSVΔG-G
314 tropism for BWMs.
315 We showed that VSVΔG-AFF-1 infects neuron and glia cells in the head (Figures S1D-
316 S1F). In order to assess the infection of other fusogen-expressing neurons, we chose the
317 arborized neuron pair PVD, previously shown to express EFF-1, which spans the length of the
318 worm [25], VSVΔG-AFF-1-infected PVD cells were not observed. Nevertheless, we found 3
319 wt animals (out of >100 infected worms), where PVD cells were infected with VSVΔG-G
320 following injections with high dosage of pseudotyped viruses (Movie S2). Moreover, we tested
321 whether ectopic AFF-1 expression in PVD or ectopic EFF-1 expression in 12 mechanosensory
322 and chemosensory neurons in *eff-1(ts)* background at the restrictive 25ºC, could induce
323 VSVΔG-AFF-1 infection in these cells. None of these treatments produced VSVΔG-AFF-1
324 infection in the neurons ectopically expressing EFF-1 or AFF-1 (Figure S3 and Table S2).
325 There are several possibilities to explain why VSVΔG-AFF-1 did not infect these neurons; (i)
326 relatively low titer of VSVΔG-AFF-1 preps, (ii) a physical barrier such as hypodermis, sheath
327 cells or glia cells that surround neurons or (iii) diffusion of the GFP signal in long neuronal
328 processes.

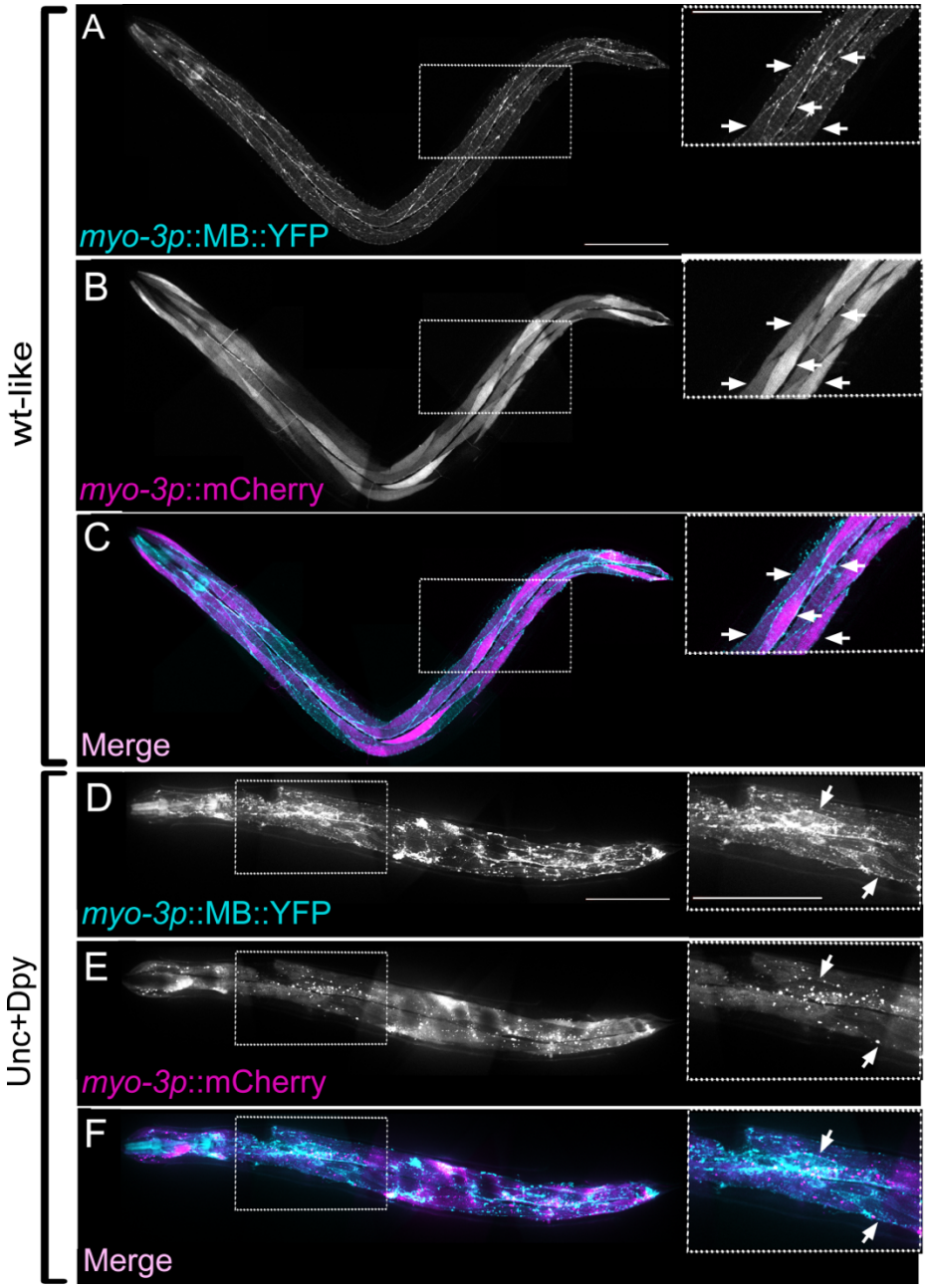


**Figure 5. EFF-1 expression in BWMs induces their fusion**

(**A-C**) Confocal images of wt-like adult worms with membrane bound (*MB*) *myo-3p::MB::YFP* (cyan) and extrachromosomal array containing *myo-3p::*EFF-1, *myo-3p::*mCherry (magenta). (**D-F**) Confocal images of Unc+Dpy [*myo-3p::MB::YFP* (cyan); *myo-3p::EFF-1*, *myo-3p::mCherry].* Arrows, unfused BWMs with MB (cyan). Note only two unfused BWMs, all the others appear fused with no MB separating them. Insets correspond to white-dotted area. Scale bars 100 µm.
See also Movie S1.

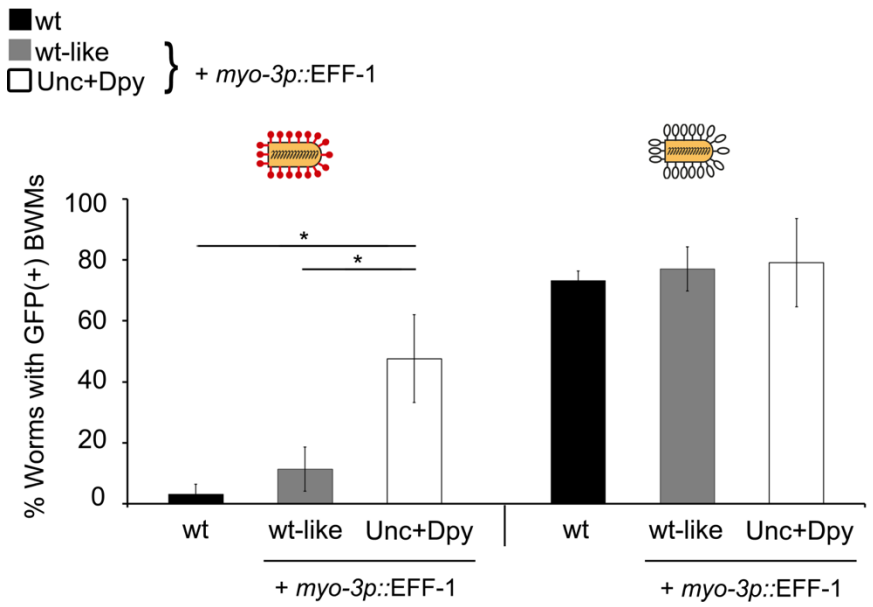


**Figure 6. Retargeting of VSVΔG-AFF-1 to body wall muscle cells**
Wild-type worms and animals with extrachromosomal array containing *myo-3p::*EFF-1 and *myo-3p::*mCherry were injected with VSVΔG-AFF-1 (35-63 IU, red pins; n=39 wt, n=50 wt-like and n=27 Unc+Dpy worms) or VSVΔG-G ($3*10^5$ IU, white pins; n=30 wt-like and 14 Unc+Dpy) respectively. Wt worms injected with VSVΔG-G (2300-4700 IU, n=56) were taken from figure 2I. Animals were analysed by SDC microscopy. Data represents average percentage of worms with GFP(+) BWMs ± SEM. Student's t-test: *p<0.05.

**EFF-1 expression in fused BWMs enables VSV∆G-AFF-1 and VSV∆G-G spreading**

Based on the aberrant muscle fusion phenotype seen in Unc+Dpy worms following EFF-1 expression in BWMs, we hypothesized that viral spreading through such novel BWM syncytia would be enhanced. To test this hypothesis, we injected VSV∆G-AFF-1 or VSV∆G-G into wt-like or Unc+Dpy worms and quantified the number of BWM cells that were either (i) mCherry(+) only (expressing EFF-1 and *myo-3p*::mCherry(+)), (ii) GFP(+) only (infected but not expressing EFF-1) or (iii) mCherry(+) and GFP(+) expression in the same cells (infected and expressing EFF-1). We found that for both VSV∆G-AFF-1 and VSV∆G-G, wt-like worms had individual GFP(+) BWM cells, that were mostly mCherry (-) (Figures 7A-7F, arrows), while Unc+Dpy animals had continuous GFP(+) BWMs that overlapped with mCherry along their body length (Figures 7G-7L, dashed lines and arrows). Compared to wt-like animals, the Unc+Dpy worms had about five-times fewer non-infected mCherry(+) only BWMs, a similar number of infected-GFP(+) only cells and about fifteen-fold more infected BWM cells that also express mCherry (Figures 7M-7N). Lastly, Unc+Dpy worms had ~2.5 nuclei per VSV∆G-AFF-1- or VSV∆G-G- infected BWMs, compared to wt-like animals with 1 nucleus per BWM cell (Figures 7O-7P). Therefore, EFF-1 expression in BWMs transforms mononucleated BWMs into syncytial muscle fibres enabling viral spreading within the fused cells and increasing the number of both VSV∆G-AFF-1- and VSV∆G-G-infected BWM cells.

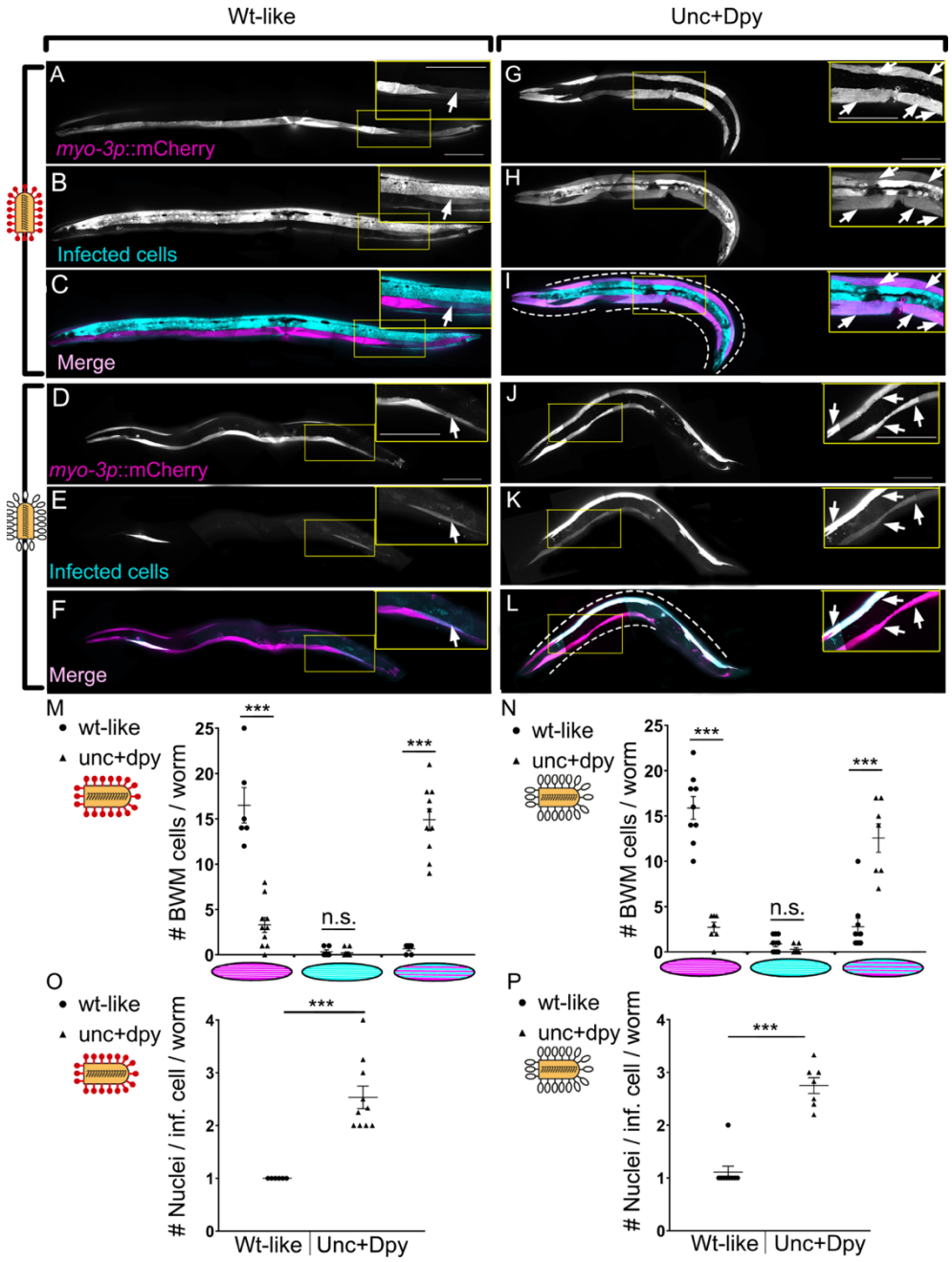


**Figure 7. EFF-1 expression in BWM enables VSVΔG-AFF-1 and VSVΔG-G spreading along fused muscles**

**(A-L)** Z-stack projections of wt-like (A-F) and Unc+Dpy animals (G-L) expressing *myo-3p::*EFF-1 and *myo-3p::*mCherry infected with VSVΔG-AFF-1 (35-63 IU red pins) or VSVΔG-G ($3*10^5$ IU; white pins). Insets and their corresponding images (yellow frames). Arrows, individual infected (cyan) BWMs. Dashed lines outline grouped BWMs that express *myo-3p*::mCherry and *myo-3p::*EFF-1 (magenta) and infected with virus (cyan) showing spreading of GFP. Scale bars, 100 µm. **(M-N)** Number of BWM cells/worm expressing EFF-1 (magenta cell), infected (cyan cell) or expressing EFF-1 and infected (magenta and cyan). wt-like (circles) and Unc+Dpy (triangles). Each point represents a single worm. **(O-P)** Quantitation of multinucleation of infected BWMs. Each dot represents an average number of nuclei/ GFP(+) BWM, calculated from 1-6 multinucleated BWMs of a single worm. (M and O) wt-like n=6 and Unc+Dpy n=10 animals. (N and P) wt-like n=9 and Unc+Dpy n=7 animals.
Black horizontal lines, average ± SEM. Student's t-test, *** p<0.0001; n.s., not-significant.

382 **Discussion**

383 **Utilizing VSV∆G-AFF-1 to study muscle fusion and muscle fusogens**

384 Myogenesis of striated muscle involves the formation of multinucleated myofibers by
385 myoblast-myoblast fusion. Myoblast fusion is also essential for muscle tissue patterning,
386 maintenance and damage repair [62,63]. In contrast, *C. elegans* BWMs do not fuse and exist
387 as mononucleated cells, contracting in synchrony that mediate gait [64]. We used VSV∆G-
388 AFF-1 to label EFF-1-expressing BWMs and found that EFF-1-mediated BWMs fusion results
389 in loss of coordination, although we did not determine whether the observed locomotory
390 defects result from aberrant joining of separately-innervated muscles or from a loss of
391 contractility. These results demonstrate that a locomotory circuit may be optimally adjusted for
392 both separate (as in *C. elegans*) and syncytial (as in vertebrate) striated muscles. Indeed,
393 failure of myoblast fusion in vertebrates may have equally severe phenotypes [47,48]. Despite
394 the importance of muscle fusion, the studies of muscle fusion proteins are just emerging [55–
395 58]. We suggest that VSV∆G-AFF-1 can be used in screens to identify additional muscle
396 fusogens in invertebrates (e.g. Drosophila). Alternatively, viruses coated with the bilateral
397 Myomaker, can be a tool to screen for muscle-expressed Myomaker-interacting proteins in
398 vertebrates.

399

400 **VSV∆G-AFF-1 infects, and can be retargeted to muscles expressing EFF-1 or AFF-1**

401 Previously described viral-vector-based systems used viral unilateral fusogens to target
402 desired cells. For instance, fusogens that are either native, modified or from different viral
403 origin, change the specificity of the viruses targets and facilitate the delivery process [1–3]. In
404 addition, a potent targeting of cancer cell lines was achieved with adenovirus (non-enveloped
405 virus) armed with an adaptor composed from 2 designed ankyrin repeat proteins (DARPins),
406 one binding to the viral fiber knob and the second binding to cancer-specific markers [44]. Our
407 work presents a new approach to retarget viral vectors into muscle cells, based on viruses
408 coated with a nematode bilateral fusogen, namely AFF-1 and expression of bilateral fusogens
409 such as EFF-1/AFF-1 in desired host cells. VSV∆G-AFF-1 has a high degree of specificity
410 towards cells that express EFF-1/AFF-1 and can be redirected by expressing them on a
411 certain cell (e.g. BWMs). Moreover, VSV∆G-AFF-1-mediated infection can be manipulated
412 quantitatively by changing the amount of a partner fusogen expressed on the target cells. VSV
413 and VSV-pseudotypes successfully infect invertebrate and vertebrate cell-lines and model
414 organisms [1,2,35–37]. Although EFF-1 and AFF-1 are not present, and have no known
415 homologs in vertebrates, VSV∆G-AFF-1 infects mammalian BHK cells expressing AFF-1/EFF-
416 1 [6]. It will be interesting to test if VSV∆G-AFF-1 can specifically target cells ectopically
417 expressing AFF-1/EFF-1 in a vertebrate model. Similarly, pseudotyped VSV∆G-SARS-CoV-

418 2-S-glycoprotein [4] could be targeted to humanized worms or mice expressing hACE2 to
419 study entry mechanisms, pathogenesis and potential treatments for viral infections, including
420 COVID19 in model organisms.
421
422 **Additional applications for VSVΔG-AFF-1**
423 In the recent decade, extracellular vesicles (EVs) emerged as intercellular communication
424 carriers, containing variable cargoes (e.g lipids, DNA, RNA, toxins and proteins) and involved
425 in different biological processes including cell-cell interactions, cancer, tissue and neuronal
426 regeneration. EVs can serve as biomarkers and are potent vehicles for gene and drug delivery
427 [26,45,46]. However, work with EVs-based vectors has to tackle the issues of specific
428 targeting, loading of desired cargo, presence of undesired/non-specific content and
429 quantification of produced EVs. Our system consisting of enveloped pseudotyped virus coated
430 with bilateral fusogens and host muscle cells expressing bilateral fusogens, demonstrates cell-
431 specific targeting. Moreover, VSVΔG-AFF-1 has the benefits of viral-based vectors, namely
432 loading a specific and tailored cargo including fluorescent markers such as GFP-coding RNA
433 sequence, simple vector quantification and cargo amplification within the host cell. Therefore,
434 VSVΔG-AFF-1 may serve as a paradigm for EVs-mediated transport. It can be utilized to
435 explore how EVs deliver their cargos and to study whether and how EVs are involved in
436 different biological processes.
437 Exoplasmic membrane fusion is a fundamental biological process involved in
438 myogenesis, fertilization, vulva development, bone formation and resorption, hypodermis
439 morphogenesis, placentation, tubulogenesis, neuronal regeneration and viral infection
440 [28,31,47,48]. Despite the importance of these processes, very few cell-cell fusogens have
441 been identified and characterized so far. These include: (i) Syncytins involved in placenta
442 formation [49–51]; (ii) Fusexins including EFF-1 and AFF-1 from *C. elegans* [14,17–22,31] and
443 HAP2/GCS1 which mediates gamete fusion in protists and flowering plants [38,52–54] and
444 (iii) Myomaker (TMEM8c) and myomerger (myomixer/minion) proteins that fuse muscle cells
445 in vertebrates [55–58]. We demonstrate that VSVΔG-AFF-1 injected into *C. elegans*
446 encounters and infects different EFF-1/AFF-1-expressing cells. Ectopic expression of EFF-1
447 in BWMs induces these mononucleated muscles to form syncytial myofibers, however, these
448 multinucleated muscles are pathological and the worms become deformed and paralyzed.
449 Moreover, bilateral heterotypic fusion has been described between EFF-1 and AFF-1 and also
450 between EFF-1 and sperm HAP2/GCS1 from *Arabidopsis* expressed on two populations of
451 BHKs [38]. Therefore, VSVΔG-AFF-1/EFF-1 may be exploited in screens to identify new
452 bilateral fusogens or fusogen-interacting proteins in different organisms and to understand

453 how and why some myoblasts fuse (e.g. skeletal muscles) while others function optimally as
454 individual mononucleated cells (e.g. smooth muscles and BWMs).
455

456 **Materials and methods**

457 **Nematode strains**

458 Unless otherwise stated, all nematodes were maintained at 20°C, according to standard
459 protocols [65,66]**.** *drh-1(tm1329)* served as the wild type background. Mutations and strains
460 that were used in this study are listed in Table S3.
461

462 **DNA constructs**

463 The *myo-3p*::EFF-1 plasmid was constructed by cloning the *myo-3* promoter region from *myo-*
464 *3p*::mCherry plasmid with Sal I (New England BioLabs Cat#R3138) and Nhe I (ThermoFisher
465 Cat# FD0974) and inserting it into the *hsp16-2*:: EFF-1 plasmid cut with the same enzymes to
466 replace the original heat shock promoter. To produce *eff-2 (hy51)* mutant worms with CRISPR,
467 the following DNA constructs were generated:

468 1. pBG115 plasmid encoding single guide targeting *eff-2* to insert *mNeonGreen* was
469 generated by cloning *eff-2* targeting sequence into the CAS9 plasmid pDD162 with BG84
470 and BG85 primers.
471 2. BG123 conversion oligonucleotide encoding wt *pha-1* fragment was PAGE purified.
472 3. PCR amplicon encoding for the mNeonGreen and unc-54 3'UTR flanked by homology
473 arms to the *eff-2* gene, generated by amplification of mNeonGreen from plasmid X, with
474 BG129 and BG130 primers containing a 50 bp homology arms to *eff-2*.

475 Sequences of primers and oligonucleotides mentioned above are found in Table S3.
476

477 **Transgenic animals**

478 For standard extrachromosomal transgenes, germline transformation was performed using
479 standard protocols [67]. Transgenic lines were kept as extrachromosomal arrays and
480 maintained by following the expression from either *myo-3p*::mCherry*, myo-2p*::GFP, or *mec-*
481 *4p*::dsRed, *odr-1p*::dsRed plasmids that were co-injected as transformation markers. *myo-*
482 *3p::*mCherry encodes mCherry expression in body wall muscle and vulva muscle cells. *myo-*
483 *2p*::GFP encodes GFP expression specifically expressed in pharyngeal muscles. *pmec-*
484 *4*::dsRed encodes dsRed expression in six touch receptor neurons. *odr-1p*::dsRed encodes
485 dsRed expression in two odor sensory neurons. Plasmids mentioned above and strains
486 containing these arrays are listed in Table S3. Transgenic lines with extrachromosomal arrays
487 were generated as follows:

488 • BP2126: *drh-1(tm1329);eff-1(hy21)* injected with 20ng/µl *pmyo-2::GFP* as
489 transformation marker and 0.1ng/µl *pdes-2::AFF-1*.
490 • BP2131-3: *drh-1(tm1329);eff-1(hy21)* injected 10ng/µl *pmec-4::dsRed* and 10ng/µl
491 *podr-1::dsRed* as transformation markers and to label sensory neurons, 1ng/µl *pmec-*
492 *4::EFF-1* and 1ng/µl *podr-1::EFF-1*.
493 • BP2137: *drh-1(tm1329)* injected 10ng/µl *myo-3p::mCherry* as transformation marker
494 and to label Body Wall Muscle cells, and 1ng/µl *myo-3p::EFF-1*.
495 *eff-2(hy51)* allele was generated by CRISPR/Cas9 [65,66] insertion of mNeonGreen into the
496 first exon of *eff-2* gene. *pha-1* was used as a conversion marker. *pha-1(e2123)* temperature
497 sensitive worms were injected with 50 ng/µl pBG115 targeting *eff-2* and containing CAS9, 50
498 ng/µl pJW1285 sgRNA plasmid against *pha-1* that contains the CAS9, 20 ng/µl BG123
499 conversion oligonucleotide encoding wt *pha-1* fragment and 20 ng/µl amplicon encoding for
500 the mNeonGreen and *unc-54* 3'UTR flanked by homology arms to the *eff-2* gene. Worms that
501 survived development at the restrictive temperature (25˚C) were screened and sequenced for
502 mutations in the *eff-2* gene. *hy51* is the result of an imprecise partial inverted insertion of the
503 PCR fragment into the *eff-2* locus. One bp was deleted at position +31 and 488bp of the unc-
504 54 3'UTR and mNeonGreen gene were inserted into *eff-2* coding region. The product of the
505 inverted insertion is a non-functional fluorescent protein that causes a frame shift in *eff-2* and
506 terminates its translation at Amino Acid #18. The *eff-2* targeting sequence was added to
507 primers (see Table S3) and inserted to the linearized vector using restriction-free cloning
508 technique.
509
510 **Live imaging of worms**
511 For imaging of viral infection and BWM fusion in *C. elegans*, worms were analyzed by
512 Nomarski optics and fluorescence microscopy using Nikon eclipse Ti inverted microscope with
513 Yokogawa CSU-X1 spinning disk confocal (SDC) as described previously [26,27]. Briefly,
514 animals were anesthetized in 0.01-0.05% tetramisole in M9 solution for 20-30 min and then
515 picked with an eyelash attached to a toothpick and transferred to a 5 µl droplet of M9 solution
516 placed on 3% agar slide. Images were acquired with Metamorph software, when using the
517 spinning disk confocal. Z-stacks were taken with Plan Fluor 40x NA=1.3 or Apochromat 60x
518 NA=1.4 objectives. Excitation of GFP was achieved with 488 nm wavelength laser (2-8%
519 intensity, 100 ms exposure time). mCherry was excited with 561 nm wavelength (15-20%
520 intensity, 100 ms exposure time). ~0.5 µm z-steps were recorded with iXon3 EMCCD camera
521 (Andor). Multidimensional data were reconstructed as maximum intensity projections using Fiji
522 software (NIH ImageJ). For live imaging of worms with fused BWM phenotypes, plates with

523 worms were placed on the stage of Zeiss stereo Discovery V8 stereo microscope. Images and
524 movies were captured at x8 magnification with additional magnification from PlanApo S 2.3X
525 objective and a Hamamatsu ORCA-ER camera controlled by micromanager software
526 (https://micro-manager.org). Figures were prepared using Fiji, Adobe Photoshop CS5 and
527 GraphPad Prism 8.
528

529 **DNA transformation and viral infection by microinjection**

530 Microinjections were performed as described [7,34] with some modifications. Shortly, late L4
531 or young adult worms were placed into droplet of halocarbon oil on 3% agarose pads. Pulled
532 capillary needles were secured onto a Nikon DIAPHOT 300 microscope equipped with a
533 micromanipulator and regulated pressure source (Narishige). For DNA transformation,
534 needles were loaded with 0.8 µl with DNA solution containing TE buffer, the target construct
535 DNA, a co-injection marker DNA and the required amount of with pKSI-1 (empty vector) DNA
536 to reach a total concentration of 100 ng/µl DNA. For experiments with viral infection, needles
537 were loaded 0.8 µl DMEM (mock-infections) or pseudo viruses in DMEM+5%FBS. Infection
538 doses of VSV are based on VSV titration on BHK cells and used 10nL volume as a single
539 microinjection dose [7]. Agar pads with worms were placed on stage of Nikon DIAPHOT 300
540 microscope. Worms were observed under x40 objective. For DNA transformation, animals
541 were injected into the gonad and immediately placed into droplet of M9 buffer placed on NGM
542 plates seeded with OP50-1 *E. coli*. For experiments with viral infection worms were injected
543 into pseudocoelom -behind the terminal bulb of the pharynx and were immediately placed into
544 droplet of M9 buffer placed on NGM plates with 50 µg/mL FUdR (Sigma), seeded with OP50-
545 1 *E. coli*. Unless otherwise stated, animals were maintained at 25°C until scoring of infection.
546

547 **Scoring viral infection**

548 Scoring viral infection using fluorescence assay was performed as described [7,34] with some
549 modifications. Briefly, 48-72 hours post injection worms were processed for live imaging as
550 described above. Animals that were unresponsive to prodding by a platinum wire worm pick
551 were considered dead and were removed from the experiment. Animals that crawled off the
552 plate or were lost during the experiment were censored. Worms with ≥1 GFP (+) cells were
553 considered as infected worms, while not injected or DMEM injected worms served as a
554 negative controls. For different experiments, either the number of GFP(+) cells/animals or the
555 type of infected tissues were observed and quantified.

556 **Temperature shift experiments**

557 Temperature sensitive *eff-1(hy21ts)* mutant worms were synchronized by hypochlorite
558 treatment of adult worms. The obtained eggs were left for overnight L1 hatching on NGM
559 plates without food at 20° C. L1 animals were then transferred to NGM plates with OP50
560 bacteria at 15° C or 25° C incubators until reaching the desired developmental stage. The
561 plates were either downshifted from 25° C to 15° C, or left at 25° C or at 15° C throughout the
562 experiment. The developmental stages were determined by analyzing gonadal size and
563 structure using Nomarski optics. Finally, worms were injected with VSV∆G-AFF-1, maintained
564 and imaged as described above.
565
566 **Counting overlapping cells**
567 To test if EFF-1 expressing BWMs were infected by VSV∆G-AFF-1, we utilized worms with an
568 extrachromosomal array expressing EFF-1 under the *myo-3* promoter and a plasmid
569 containing *myo-3p*::mCherry. We found that most mCherry (+) worms had a wt-like phenotype,
570 but a small fraction of these worms were Unc+Dpy. Importantly, all sibling mCherry(-) worms
571 were wt-like (Table S1). Hence, for the experiment we utilized a fluorescence
572 stereomicroscope and chose late L4/ young adult, wt-like and Unc+Dpy animals that had
573 continuous *myo-3p::mCherry*(+) BWMs (which could express EFF-1 and fuse with each other).
574 Next, these worms were injected with VSV∆G-AFF-1 or VSV∆G-G. 48-72h later, Z-stack
575 images of the worms were obtained with SDC microscope (as described in live imaging
576 section). Worms with ≥1 infected BWM were selected. For each worm, we counted the number
577 of BWMs that were mCherry(+) only ( express EFF-1), GFP(+) only (infected by virus) and
578 overlapping- with both mCherry(+) and GFP(+) (express EFF-1 and infected).
579
580 **Counting number of nuclei per BWM**
581 To test if ectopic EFF-1 expression in BWMs produces multinucleated BWMs, wt-like and
582 Unc+Dpy animals that had continuous *myo-3p::mCherry*(+) BWMs (which could express EFF-
583 1 and fuse with each other) were imaged by SDC microscope as described above. In one set
584 of experiments we imaged L2 worms and counted number of nuclei per *myo-3p::mCherry* cell.
585 In a second set of experiments, we imaged adult worms with BWMs infected by either VSV∆G-
586 AFF-1 or VSV∆G-G and counted number of nuclei per infected (GFP(+)) BWM cell. For both
587 sets of experiments, in worms with at least one multinucleated BWM we monitored all
588 multinucleated BWMs and calculated the average number of nuclei/BWM for each worm.
589 Worms in which multinucleated cells were not observed, were considered as having 1
590 nucleus/BWM.
591
592 **Counting phenotypes in worms expressing EFF-1 in BWMs**

593 To find whether ectopic expression of EFF-1 in BWM cells produces any special phenotypes,
594 we used BP2137 *drh-1(tm1329)IV*; hyEx375[*myo-3p*::EFF-1, *myo-3p*::mCherry, KS
595 bluescript]. We first isolated 4 wt-like *myo-3p::mCherry* L4 hermaphrodite worms, one worm
596 per NGM plate+Op50. These worms were led to lay eggs and were transferred to a fresh
597 plate 1-2 times per day during 5 days. Progeny including eggs, larvae and adults were divided
598 into two groups, namely *myo-3p::mCherry*(+) and *myo-3p::mCherry*(-). We counted the total
599 number of progeny with a certain phenotype (e.g. wt-like worms, adult Unc+Dpy worms, larval
600 arrested Unc+Dpy worms and unhatched eggs) for each of the 4 mothers. Finally, we
601 calculated the average number of worms with certain phenotype ± SEM and the fraction ± SE
602 of worms with a certain phenotype in each group.
603
604 **Cell culture and preparation of pseudoviruses**
605 Baby Hamster Kidney cells (BHK), BHK-21(ATCC) were cultured in Dulbecco's Modified
606 Eagles Medium (DMEM) and recombinant viruses were prepared as described [6] with some
607 modifications. Briefly, BHK cells were grown to 70% confluence on 10 cm plates and then
608 transfected using Fugene HD + OptiMEM at ratio 1:4 (Fugene:DNA), with plasmids encoding
609 pOA20 (pCAGGS::*aff-1*::FLAG, 2µg/ml final concentration) [6] or pOA28 (pCAGGS::VSV-G
610 Indiana, 1µg/ml final concentration)[33]. Following 24 h incubation at 37°C in 5% $CO_2$, cells
611 were infected with VSVG-complemented VSV∆G recombinant virus (VSV∆G-G) at a
612 multiplicity of infection (MOI) of 5, for 1 hour at 37°C in a 5% $CO_2$ incubator in serum free
613 DMEM. Virus infected cells were washed 3-6 times with PBS (+ $Ca^{++}$ & $Mg^{++}$) to remove
614 unabsorbed VSV∆G-G virus. Following a 24 h incubation period at 37°C, the supernatant
615 containing the VSV∆G-G, or VSV∆G-AFF-1 pseudoviruses were harvested without scraping
616 the cells and centrifuged at 600 g for 10 min at 4°C to clear cell debris. VSV∆G-AFF-1 Virions
617 were filtered through 0.22 µm filter unit and then double concentrated. First, by pelleting at
618 100,000 g through a 20% sucrose cushion, and resuspension in 10%FBS DMEM, second, by
619 pelleting at 100,000 g through a 10% sucrose cushion, and final resuspension in 45µl DMEM.
620 Finally, VSV∆G-AFF-1 was incubated with anti-VSV-G antibody mAb diluted 1:1000 to inhibit
621 infection due to residual presence of VSV-G. The effective blocking of VSV-G was confirmed
622 by tittering pseudoviruses in BHK cells and by injection of VSV∆G-G incubated with anti-VSV-
623 G into worms (Figure S4).
624
625 **Titering VSV pseudotyped viruses**
626 Titering VSV pseudotyped viruses was performed as described [6] with some modifications.
627 Briefly, $5x10^3$ BHK cells were plated into each well of a 96 well tissue culture plate (NUNC,
628 cat# 167008). To determine the titer of VSV∆G-AFF-1, BHK cells were initially transfected with

629 2 µg/ml pOA20 (pCAGGS::AFF-1::FLAG). Cells transfected with empty vector served as
630 control. Eight serial x2 dilutions of the virus were performed and added to cells. After 18-24
631 hours of incubation, GFP expressing cells were counted in at least three dilutions using x20
632 objective of Zeiss Axiovert 200M fluorescence microscope. Inoculation was performed in the
633 presence of anti-VSV-G antibody mAb diluted 1:1000 to inhibit infection due to residual
634 presence of VSV-G.
635
636 **Statistical tests**
637 The specific tests used are described in the figure captions and the results section. The graphs
638 show mean ± SEM unless noted otherwise. For each experiment at least two biological
639 replicates were performed and the number of animals per experiment is stated in the figure
640 legends.
641

642 **References**


643 1. Lichty, B.D., Power, A.T., Stojdl, D.F., and Bell, J.C. (2004). Vesicular stomatitis virus:
644 Re-inventing the bullet. Trends Mol. Med. *10*, 210–216.
645 2. van den Pol, A.N., Ozduman, K., Wollmann, G., Ho, W.S.C., Simon, I., Yao, Y., Rose,
646 J.K., and Ghosh, P. (2009). Viral strategies for studying the brain, including a
647 replication-restricted self-amplifying delta-G vesicular stomatis virus that rapidly
648 expresses transgenes in brain and can generate a multicolor Golgi-like expression. J.
649 Comp. Neurol. *516*, 456–481.
650 3. Hastie, E., Cataldi, M., Marriott, I., and Grdzelishvili, V.Z. (2013). Understanding and
651 altering cell tropism of vesicular stomatitis virus. Virus Res. *176*, 16–32.
652 4. Hoffmann, M., Kleine-Weber, H., Schroeder, S., Krüger, N., Herrler, T., Erichsen, S.,
653 Schiergens, T.S., Herrler, G., Wu, N.-H., Nitsche, A., *et al.* (2020). SARS-CoV-2 Cell
654 Entry Depends on ACE2 and TMPRSS2 and Is Blocked by a Clinically Proven Protease
655 Inhibitor. Cell *181*, 271–280.
656 5. Halperin, S.A., Das, R., Onorato, M.T., Liu, K., Martin, J., Grant-Klein, R.J., Nichols, R.,
657 Coller, B.-A., Helmond, F.A., and Simon, J.K. (2019). Immunogenicity, Lot Consistency,
658 and Extended Safety of rVSVΔG-ZEBOV-GP Vaccine: A Phase 3 Randomized,
659 Double-Blind, Placebo-Controlled Study in Healthy Adults. J. Infect. Dis. *220*, 1127–
660 1135.
661 6. Avinoam, O., Fridman, K., Valansi, C., Abutbul, I., Zeev-Ben-Mordehai, T., Maurer,
662 U.E., Sapir, A., Danino, D., Grünewald, K., White, J.M., *et al.* (2011). Conserved
663 eukaryotic fusogens can fuse viral envelopes to cells. Science. *332*, 589–592.
664 7. Gammon, D.B., Ishidate, T., Li, L., Gu, W., Silverman, N., and Mello, C.C. (2017). The
665 Antiviral RNA Interference Response Provides Resistance to Lethal Arbovirus Infection
666 and Vertical Transmission in Caenorhabditis elegans. Curr. Biol. *27*, 795–806.
667 8. Presley, J.F., Smith, C., Hirschberg, K., Miller, C., Cole, N.B., Zaal, K.J.M., and
668 Lippincott-Schwartz, J. (1998). Golgi membrane dynamics. Mol. Biol. Cell *9*, 1617–
669 1626.
670 9. Ogino, T., and Green, T.J. (2019). RNA Synthesis and Capping by Non-segmented
671 Negative Strand RNA Viral Polymerases: Lessons From a Prototypic Virus. Front.
672 Microbiol. *10*, 1490.
673 10. Finkelshtein, D., Werman, A., Novick, D., Barak, S., and Rubinstein, M. (2013). LDL
674 receptor and its family members serve as the cellular receptors for vesicular stomatitis
675 virus. Proc. Natl. Acad. Sci. U. S. A. *110*, 7306–7311.
676 11. Bergman, I., Whitaker-Dowling, P., Gao, Y., Griffin, J.A., and Watkins, S.C. (2003).
677 Vesicular stomatitis virus expressing a chimeric Sindbis glycoprotein containing an Fc
678 antibody binding domain targets to Her2/neu overexpressing breast cancer cells.
679 Virology *316*, 337–347.
680 12. Schnell, M.J., Johnson, J.E., Buonocore, L., and Rose, J.K. (1997). Construction of a
681 novel virus that targets HIV-1-infected cells and controls HIV-1 infection. Cell *90*, 849–
682 857.
683 13. Gao, Y., Whitaker-Dowling, P., Griffin, J.A., Barmada, M.A., and Bergman, I. (2009).
684 Recombinant vesicular stomatitis virus targeted to Her2/neu combined with anti-CTLA4
685 antibody eliminates implanted mammary tumors. Cancer Gene Ther. *16*, 44–52.
686 14. Mohler, W.A., Shemer, G., Del Campo, J.J., Valansi, C., Opoku-Serebuoh, E.,
687 Scranton, V., Assaf, N., White, J.G., and Podbilewicz, B. (2002). The type 1 membrane
688 protein EFF-1 is essential for development cell fusion. Dev. Cell *2*, 355–362.
689 15. Shemer, G., and Podbilewicz, B. (2002). LIN-39/Hox triggers cell division and
690 represses EFF-1/fusogen-dependent vulval cell fusion. Genes Dev.
691 16. Podbilewicz, B. (2006). Cell fusion. WormBook *93*, 71–79.
692 17. Rasmussen, J.P., English, K., Tenlen, J.R., and Priess, J.R. (2008). Notch Signaling
693 and Morphogenesis of Single-Cell Tubes in the C. elegans Digestive Tract. Dev. Cell
694 *14*, 559–569.

18. Sapir, A., Choi, J., Leikina, E., Avinoam, O., Valansi, C., Chernomordik, L. V., Newman, A.P., and Podbilewicz, B. (2007). AFF-1, a FOS-1-Regulated Fusogen, Mediates Fusion of the Anchor Cell in C. elegans. Dev. Cell *12*, 683–698.
19. Shemer, G., Suissa, M., Kolotuev, I., Nguyen, K.C.Q., Hall, D.H., and Podbilewicz, B. (2004). EFF-1 is sufficient to initiate and execute tissue-specific cell fusion in C. elegans. Curr. Biol. *14*, 1587–1591.
20. Abdus-Saboor, I., Mancuso, V.P., Murray, J.I., Palozola, K., Norris, C., Hall, D.H., Howell, K., Huang, K., and Sundaram, M. V. (2011). Notch and Ras promote sequential steps of excretory tube development in C. elegans. Development *138*, 3545–3555.
21. Soulavie, F., Hall, D.H., and Sundaram, M. V. (2018). The AFF-1 exoplasmic fusogen is required for endocytic scission and seamless tube elongation. Nat. Commun. *9*, 1741.
22. Stone, C.E., Hall, D.H., and Sundaram, M. V. (2009). Lipocalin signaling controls unicellular tube development in the Caenorhabditis elegans excretory system. Dev. Biol. *329*, 201–211.
23. Ghosh-Roy, A., Wu, Z., Goncharov, A., Jin, Y., and Chisholm, A.D. (2010). Calcium and cyclic AMP promote axonal regeneration in Caenorhabditis elegans and require DLK-1 kinase. J. Neurosci. *30*, 3175–3183.
24. Neumann, B., Coakley, S., Giordano-Santini, R., Linton, C., Lee, E.S. eun., Nakagawa, A., Xue, D., and Hilliard, M.A. (2015). EFF-1-mediated regenerative axonal fusion requires components of the apoptotic pathway. Nature *517*, 219–222.
25. Oren-Suissa, M., Hall, D.H., Treinin, M., Shemer, G., and Podbilewicz, B. (2010). The fusogen EFF-I controls sculpting of mechanosensory dendrites. Science. *328*, 1285–1288.
26. Oren-Suissa, M., Gattegno, T., Kravtsov, V., and Podbilewicz, B. (2017). Extrinsic repair of injured dendrites as a paradigm for regeneration by fusion in Caenorhabditis elegans. Genetics *206*, 215–230.
27. Kravtsov, V., Oren-Suissa, M., and Podbilewicz, B. (2017). The fusogen AFF-1 can rejuvenate the regenerative potential of adult dendritic trees by self-fusion. Dev. *144*, 2364–2374.
28. Harrison, S.C. (2015). Viral membrane fusion. Virology *479–480*, 498–507.
29. Podbilewicz, B. (2014). Virus and Cell Fusion Mechanisms. Annu. Rev. Cell Dev. Biol. *30*, 111–139.
30. Pérez-Vargas, J., Krey, T., Valansi, C., Avinoam, O., Haouz, A., Jamin, M., Raveh-Barak, H., Podbilewicz, B., and Rey, F.A. (2014). Structural basis of eukaryotic cell-cell fusion. Cell *157*, 407–419.
31. White, J.M. (2007). The First Family of Cell-Cell Fusion. Dev. Cell *12*, 683–698.
32. Robison, C.S., and Whitt, M.A. (2000). The Membrane-Proximal Stem Region of Vesicular Stomatitis Virus G Protein Confers Efficient Virus Assembly. J. Virol. *74*, 2239–2246.
33. Whitt, M.A. (2010). Generation of VSV pseudotypes using recombinant ΔG-VSV for studies on virus entry, identification of entry inhibitors, and immune responses to vaccines. J. Virol. Methods *169*, 365–374.
34. Martin, A., Rex, E., Ishidate, T., Lin, R., and Gammon, D. (2017). Infection of Caenorhabditis elegans with Vesicular Stomatitis Virus via Microinjection. BIO-PROTOCOL *7*, e2617.
35. Quiroz, E., Moreno, N., Peralta, P.H., and Tesh, R.B. (1988). A human case of encephalitis associated with vesicular stomatitis virus (Indiana serotype) infection. Am. J. Trop. Med. Hyg. *39*, 312–314.
36. Guerra-Varela, J., Baz-Martínez, M., Da Silva-Álvarez, S., Losada, A.P., Quiroga, M.I., Collado, M., Rivas, C., and Sánchez, L. (2018). Susceptibility of Zebrafish to Vesicular Stomatitis Virus Infection. Zebrafish *15*, 124–132.
37. Barrera, J.D.C., and Letchworth, G.J. (1996). Persistence of Vesicular Stomatitis Virus

New Jersey RNA in Convalescent Hamsters. Virology *219*, 453–464.
38. Valansi, C., Moi, D., Leikina, E., Matveev, E., Graña, M., Chernomordik, L. V., Romero, H., Aguilar, P.S., and Podbilewicz, B. (2017). Arabidopsis HAP2/GCS1 is a gamete fusion protein homologous to somatic and viral fusogens. J. Cell Biol. *216*, 571–581.
39. Yochem, J., Gu, T., and Han, M. (1998). A new marker for mosaic analysis in Caenorhabditis elegans indicates a fusion between hyp6 and hyp7, two major components of the hypodermis. Genetics *149*, 1323–1334.
40. Podbilewicz, B., and White, J.G. (1994). Cell fusions in the developing epithelia of C. elegans. Dev. Biol. *161*, 408–424.
41. Fukushige, T., Brodigan, T.M., Schriefer, L.A., Waterston, R.H., and Krause, M. (2006). Defining the transcriptional redundancy of early bodywall muscle development in C. elegans: Evidence for a unified theory of animal muscle development. Genes Dev. *20*, 3395–3406.
42. Kim, J., Löwe, T., and Hoppe, T. (2008). Protein quality control gets muscle into shape. Trends Cell Biol. *18*, 264–272.
43. Frumkin, A., Dror, S., Pokrzywa, W., Bar-Lavan, Y., Karady, I., Hoppe, T., and Ben-Zvi, A. (2014). Challenging muscle homeostasis uncovers novel chaperone interactions in Caenorhabditis elegans. Front. Mol. Biosci. *6*, 21.
44. Dreier, B., Honegger, A., Hess, C., Nagy-Davidescu, G., Mittl, P.R.E., Grütter, M.G., Belousova, N., Mikheeva, G., Krasnykh, V., and Plückthun, A. (2013). Development of a generic adenovirus delivery system based on structure-guided design of bispecific trimeric DARPin adapters. Proc. Natl. Acad. Sci. U. S. A. *5*, E869–E877.
45. Raposo, G., and Stoorvogel, W. (2013). Extracellular vesicles: Exosomes, microvesicles, and friends. J. Cell Biol. *200*, 373–383.
46. Sdrimas, K., and Kourembanas, S. (2014). MSC microvesicles for the treatment of lung disease: A new paradigm for cell-free therapy. Antioxidants Redox Signal. *21*, 1905–1915.
47. Segev, N., Avinoam, O., and Podbilewicz, B. (2018). Fusogens. Curr. Biol. *28*, R378-R380.
48. Brukman, N.G., Uygur, B., Podbilewicz, B., and Chernomordik, L. V. (2019). How cells fuse. J. Cell Biol. *218*, 1436–1451.
49. Blond, J.-L., Lavillette, D., Cheynet, V., Bouton, O., Oriol, G., Chapel-Fernandes, S., Mandrand, B., Mallet, F., and Cosset, F.-L. (2000). An Envelope Glycoprotein of the Human Endogenous Retrovirus HERV-W Is Expressed in the Human Placenta and Fuses Cells Expressing the Type D Mammalian Retrovirus Receptor. J. Virol. *74*, 3321–3329.
50. Sha, M., Lee, X., Li, X. ping, Veldman, G.M., Finnerty, H., Racie, L., LaVallie, E., Tang, X.Y., Edouard, P., Howes, S., *et al.* (2000). Syncytin is a captive retroviral envelope protein involved in human placental morphogenesis. Nature *403*, 785–789.
51. Kokkinos, M.I., Murthi, P., Wafai, R., Thompson, E.W., and Newgreen, D.F. (2010). Cadherins in the human placenta - Epithelial-mesenchymal transition (EMT) and placental development. Placenta *31*, 747–755.
52. von Besser, K., Frank, A.C., Johnson, M.A., and Preuss, D. (2006). Arabidopsis HAP2 (GCS1) is a sperm-specific gene required for pollen tube guidance and fertilization. Development *133*, 4761–4769.
53. Liu, C., Zhou, Y., Zhang, X., Zhang, J., Zhou, Z., Weng, J., Li, X., and Wang, Z. (2019). Natural variation in the THICK TASSEL DWARF1 (TD1) gene in the regulation of maize (Zea mays L.) ear-related traits. Breed. Sci. *69*, 323–331.
54. Cole, E.S., Cassidy-Hanley, D., Fricke Pinello, J., Zeng, H., Hsueh, M., Kolbin, D., Ozzello, C., Giddings, T., Winey, M., and Clark, T.G. (2014). Function of the male-gamete-specific fusion protein HAP2 in a seven-sexed ciliate. Curr. Biol. *24*, 2168–2173.
55. Millay, D.P., O'Rourke, J.R., Sutherland, L.B., Bezprozvannaya, S., Shelton, J.M.,

Bassel-Duby, R., and Olson, E.N. (2013). Myomaker is a membrane activator of myoblast fusion and muscle formation. Nature *499*, 301–305.

56. Gamage, D.G., Leikina, E., Quinn, M.E., Ratinov, A., Chernomordik, L. V., and Millay, D.P. (2017). Insights into the localization and function of myomaker during myoblast fusion. J. Biol. Chem. *292*, 17272–17289.
57. Mitani, Y., Vagnozzi, R.J., and Millay, D.P. (2017). In vivo myomaker-mediated heterologous fusion and nuclear reprogramming. FASEB J. *31*, 400–411.
58. Bi, P., Ramirez-Martinez, A., Li, H., Cannavino, J., McAnally, J.R., Shelton, J.M., Sánchez-Ortiz, E., Bassel-Duby, R., and Olson, E.N. (2017). Control of muscle formation by the fusogenic micropeptide myomixer. Science (80-. ). *356*, 323–327.
59. Zhu, T., Liang, X., Wang, X.M., and Shen, K. (2017). Dynein and EFF-1 control dendrite morphology by regulating the localization pattern of SAX-7 in epidermal cells. J. Cell Sci. *130*, 4063–4071.
60. Buechner, M., Hall, D.H., Bhatt, H., and Hedgecock, E.M. (1999). Cystic canal mutants in Caenorhabditis elegans are defective in the apical membrane domain of the renal (excretory) cell. Dev. Biol. *214*, 227–241.
61. Nelson, F.K., and Riddle, D.L. (1984). Functional study of the Caenorhabditis elegans secretory-excretory system using laser microsurgery. J. Exp. Zool. *231*, 45–56.
62. Gunage, R.D., Dhanyasi, N., Reichert, H., and VijayRaghavan, K. (2017). Drosophila adult muscle development and regeneration. Semin. Cell Dev. Biol. *72*, 56–66.
63. Sampath, S.C., Sampath, S.C., and Millay, D.P. (2018). Myoblast fusion confusion: The resolution begins. Skelet. Muscle *8*, 3.
64. Gjorgjieva, J., Biron, D., and Haspel, G. (2014). Neurobiology of caenorhabditis elegans locomotion: Where do we stand? Bioscience, 476–486.
65. Brenner, S. (1974). The genetics of Caenorabditis elegans. Genetics *77*, 71–94.
66. Sulston, J., and Hodgkin, J. (1988). Methods in the nematode C. elegans. In Cold Spring Harbor Laboratory Press, pp. 587–606.
67. Mello, C., and Fire, A. (1995). DNA Transformation. Methods Cell Biol. *8*, 2159–2165.
68. Takada, A., Robison, C., Goto, H., Sanchez, A., Murti, K.G., Whitt, M.A., and Kawaoka, Y. (1997). A system for functional analysis of Ebola virus glycoprotein. Proc Natl Acad Sci U S A *94*, 14764-14769.
69. Stoker, M., and Macpherson, I. (1964). Syrian Hamster Fibroblast Cell Line Bhk21 and Its Derivatives. Nature *203*, 1355-1357.
70. Diaz-Balzac, C.A., Rahman, M., Lazaro-Pena, M.I., Martin Hernandez, L.A., Salzberg, Y., Aguirre-Chen, C., Kaprielian, Z., and Bulow, H.E. (2016). Muscle- and Skin-Derived Cues Jointly Orchestrate Patterning of Somatosensory Dendrites. Curr Biol *26*, 2397.
71. Yang, J., Sun, B., Huang, H., Jiang, Y., Diao, L., Chen, B., Xu, C., Wang, X., Liu, J., Jiang, W., et al. (2014). High-efficiency scarless genetic modification in Escherichia coli by using lambda red recombination and I-SceI cleavage. Appl Environ Microbiol *80*, 3826-3834.
72. Frokjaer-Jensen, C., Davis, M.W., Hopkins, C.E., Newman, B.J., Thummel, J.M., Olesen, S.P., Grunnet, M., and Jorgensen, E.M. (2008). Single-copy insertion of transgenes in Caenorhabditis elegans. Nat Genet *40*, 1375-1383.
73. Dickinson, D.J., Ward, J.D., Reiner, D.J., and Goldstein, B. (2013). Engineering the Caenorhabditis elegans genome using Cas9-triggered homologous recombination. Nat Methods *10*, 1028-1034.
74. Ward, J.D. (2015). Rapid and precise engineering of the Caenorhabditis elegans genome with lethal mutation co-conversion and inactivation of NHEJ repair. Genetics *199*, 363-377.
75. Edelstein, A., Amodaj, N., Hoover, K., Vale, R., and Stuurman, N. (2010). Computer control of microscopes using microManager. Curr Protoc Mol Biol *Chapter 14*, Unit14 20.

854 **Abbreviations**

855 AFF-1 Anchor cell Fusion Failure
856 BHK Baby Hamster Kidney cells
857 BWM Body Wall Muscle
858 Dpy Dumpy phenotype
859 EC Excretory Canal cell
860 EFF-1 Epithelial Fusion Failure 1
861 EFF-2 Epithelial Fusion Failure 2
862 FUSEXINS FUSion proteins essential for sexual reproduction and Exoplasmic merger of
863 plasma membranes
864 HYP Hypodermis (epidermis)
865 SM Somatointestinal Muscle
866 ts temperature sensitive
867 UM Uterine Muscle
868 Unc Uncoordinated phenotype
869 VSV Vesicular Stomatitis Virus
870 VSV-G VSV-glycoprotein G
871 VSVΔG pseudoviruses in which the glycoprotein G gene was deleted
872 VSVΔG-AFF-1 pseudovirus coated with AFF-1
873 VSVΔG-G pseudovirus coated with G glycoprotein
874

875 **Acknowledgements**

876 We thank Don Gammon for providing the *drh-1(-)* worms, Massimo Hilliard for providing *mec-*
877 *4p*::mCherry, *mec-4p*::EFF-1, *odr-1p*::dsRed and *odr-1p*::EFF-1 plasmids and the
878 Caenorhabditis Genetics Center for nematode strains. We thank Andy Fire for suggesting
879 studying syncytial BWMs and their potential phenotypes. We also thank Sharon Inberg, Yael
880 Iosilevskii, Rosina Giordano-Santini, Dan Cassel and Sivan Korenblit for helpful discussions
881 and for critically reading the manuscript.
882

883 **Author contributions**

884 A.M. and B.P. conceived the project. A.M. performed all experiments unless otherwise
885 specified. X.L. generated *myo-3p*::EFF-1 Plasmid and BP2171-3 nematode strains and
886 performed imaging of worms in Figure 5. E.M. improved viral preparation protocol. B.G.
887 generated EFF-2 CRISPR plasmid and O.K. produced *eff-2(hy51)* worms. A.M. and B.P
888 analyzed data and wrote the manuscript, with input from all authors.
889

890 **Online supplemental material**

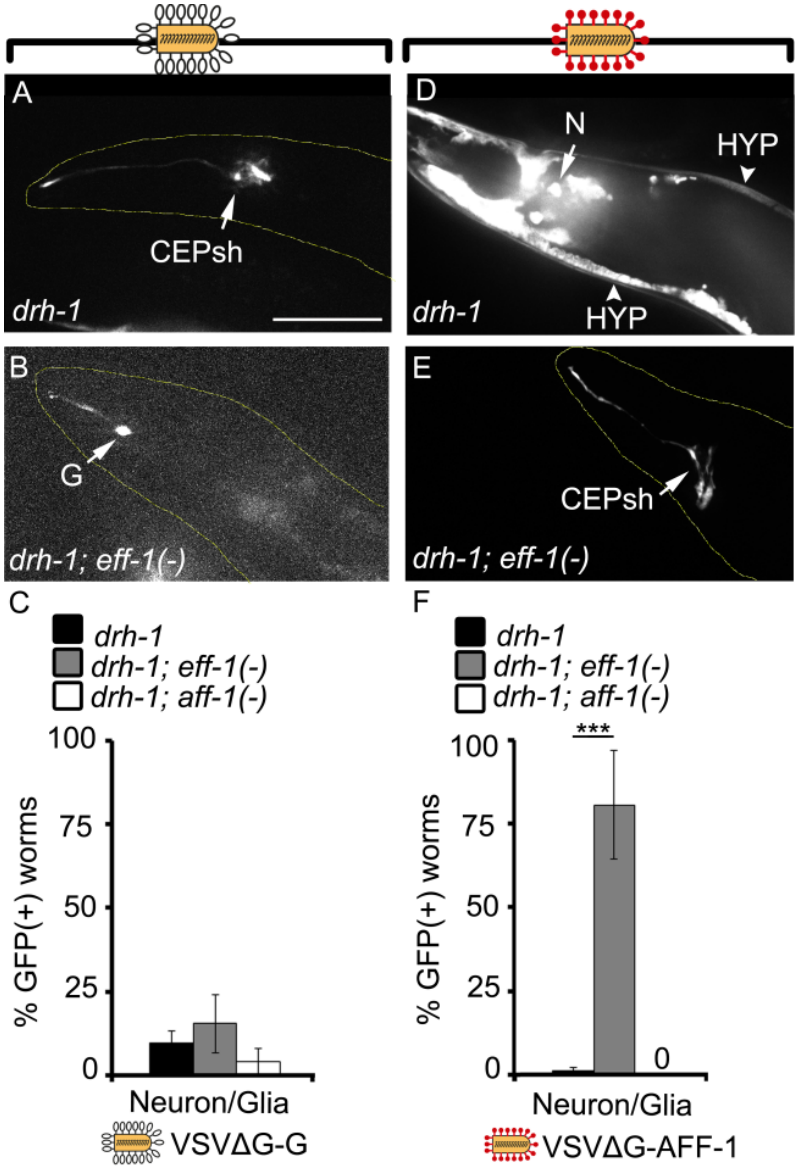


891

892

893 **Figure S1: VSVΔG-AFF-1 and VSVΔG-G infect glia and neuron cells**

894 **(A-B)** SDC microscope Z-stack projections of *drh-1* and *drh-1; eff-1(-)* worms injected in the
895 pseudocoelom with 2300-4700 IU VSVΔG-G (white pins) and their heads imaged 48 h later.
896 **(C)** Fraction of GFP(+) worms infected with VSVΔG-G in neuron/glia cells in the specified
897 background. Animals were injected with VSVΔG-G and analyzed as in (A-B).
898 **(D-E)** SDC microscope Z-stack projections of *C. elegans* cells infected with 33-240 IU VSVΔG-
899 AFF-1 (red pins). *drh-1* or *drh-1; eff-1(-)* worms were injected in the pseudocoelom and
900 imaged 48 h later.
901 **(F)** Fraction of GFP(+) worms infected with VSVΔG-AFF-1 in neuron/glia cells. Animals were
902 analyzed as in (D-E). For (A-B) and (D-E) arrowheads point to hypodermal nuclei (HYP) and
903 arrows point to indicated infected cell. CEPsh- Cephalic Sheath (glia), G- glia, N- neuron.
904 Scale bar, 50 µm. In (A, B and E) yellow dashed lines outline worm's anterior body (head). In
905 (C) and (F), bars represent average ± SEM. ***P<0.001 (Student's T- test). For VSVΔG-AFF-
906 1: n=46,15 and 10 for *drh-1*,*drh-1;eff-1(-)* and *drh-1;aff-1(-)* respectively, and for VSVΔG-G:
907 n= 56, 39 and 15 for *drh-1*, *drh-1;eff-1(-)* and *drh-1;aff-1(-)* respectively).

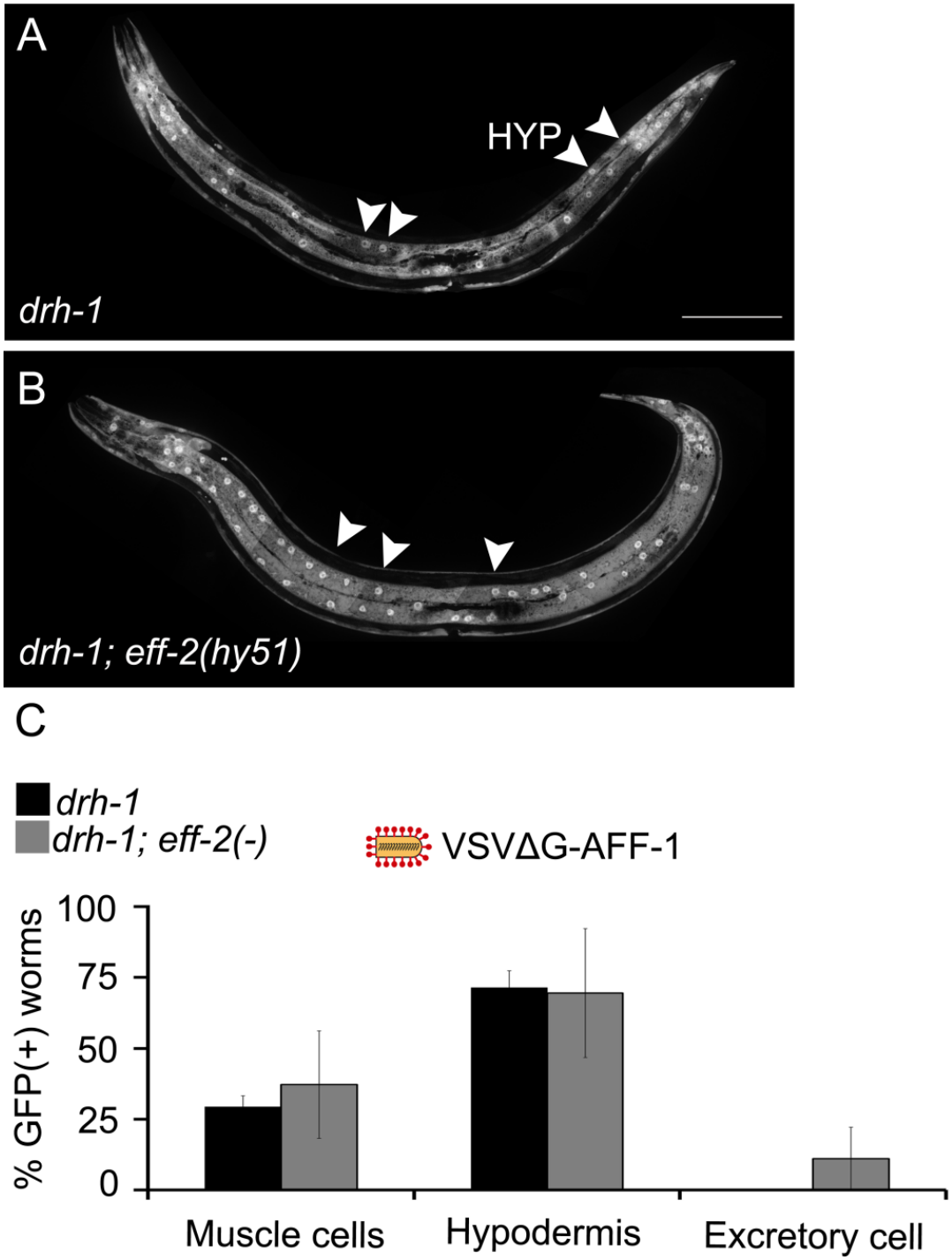


**Figure S2: VSVΔG-AFF-1 infects *eff-2(-)* worms**

**(A-B)** SDC microscope Z-stack projections of *drh-1* or *drh-1;eff-2(-)* worms injected with VSVΔG-AFF-1 (35-67 IU) and imaged 48 h later.
**(C)** Fraction of GFP(+) worms infected with VSVΔG-AFF-1. Animals were injected with VSVΔG-AFF-1 and analyzed as in (A-B). Arrowheads point to hypodermal (HYP) nuclei. Scale bar, 100 µm. In (C) bars represent average ± SEM. n=23 and 20 for *drh-1* and *drh-1;eff-2(-)* respectively. For all types of infected cells, there is no significant difference between % GFP(+) worms from *drh-1* and *drh-1;eff-2 (-)* backgrounds with two-tailed Student's t-test ($p<0.05$).

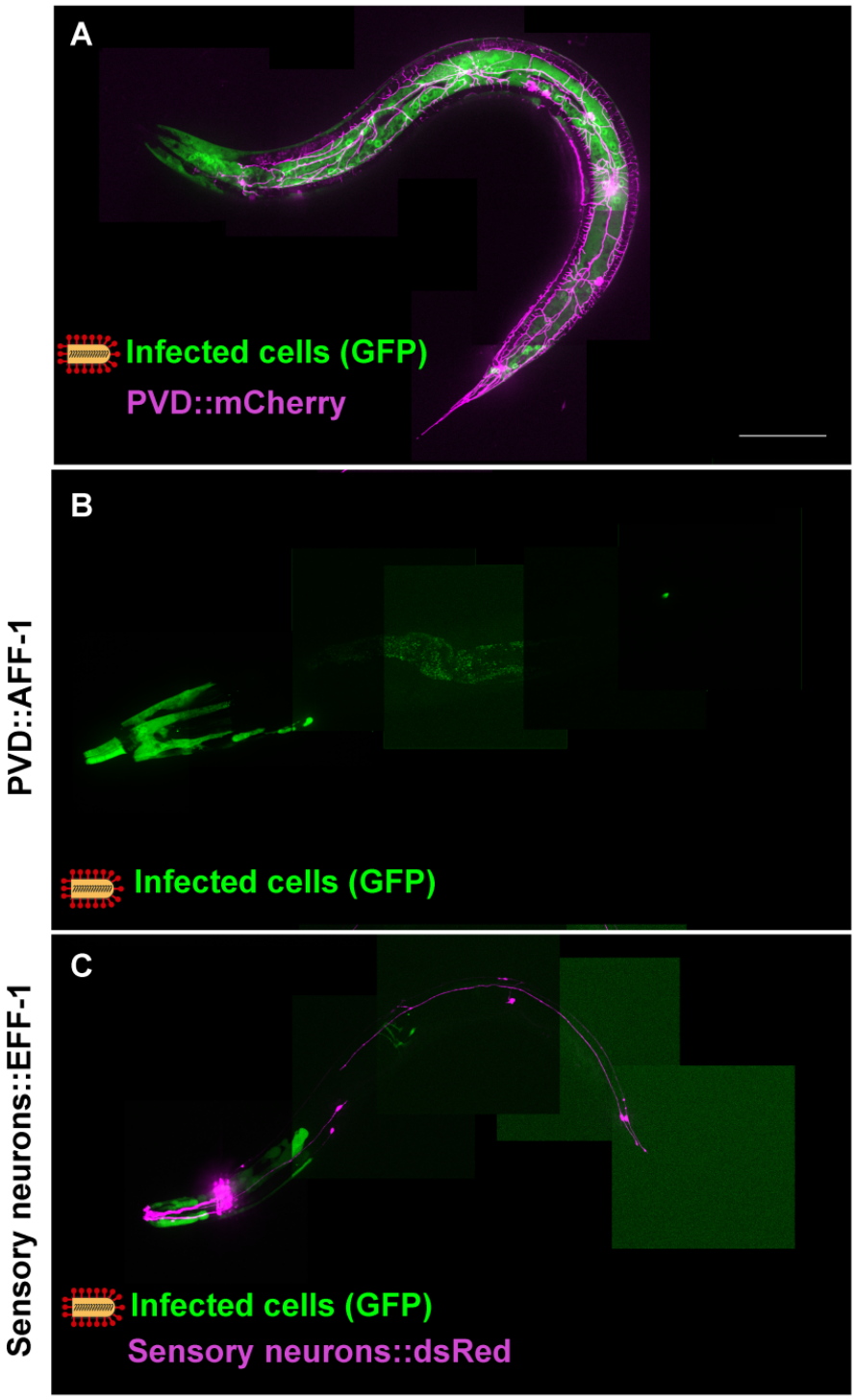


**Figure S3. VSVΔG-AFF-1 does not infect PVD and other sensory neurons ectopically expressing AFF-1/EFF-1**

**(A-C)** SDC microscope Z-stack projections of animals infected with 82-103 IU VSVΔG-AFF-1 (red pins). (For genotypes and quantitation see Table S2). Scale bar, 100 µm.

(**A**) Young adult expressing mCherry in PVD.

(**B**) *eff-1(ts)* adult expressing AFF-1 in PVD.

(**C**) *eff-1(ts)* adult expressing EFF-1 and dsRed in 12 sensory neurons.

See also Table S2 and Movie S2.

929

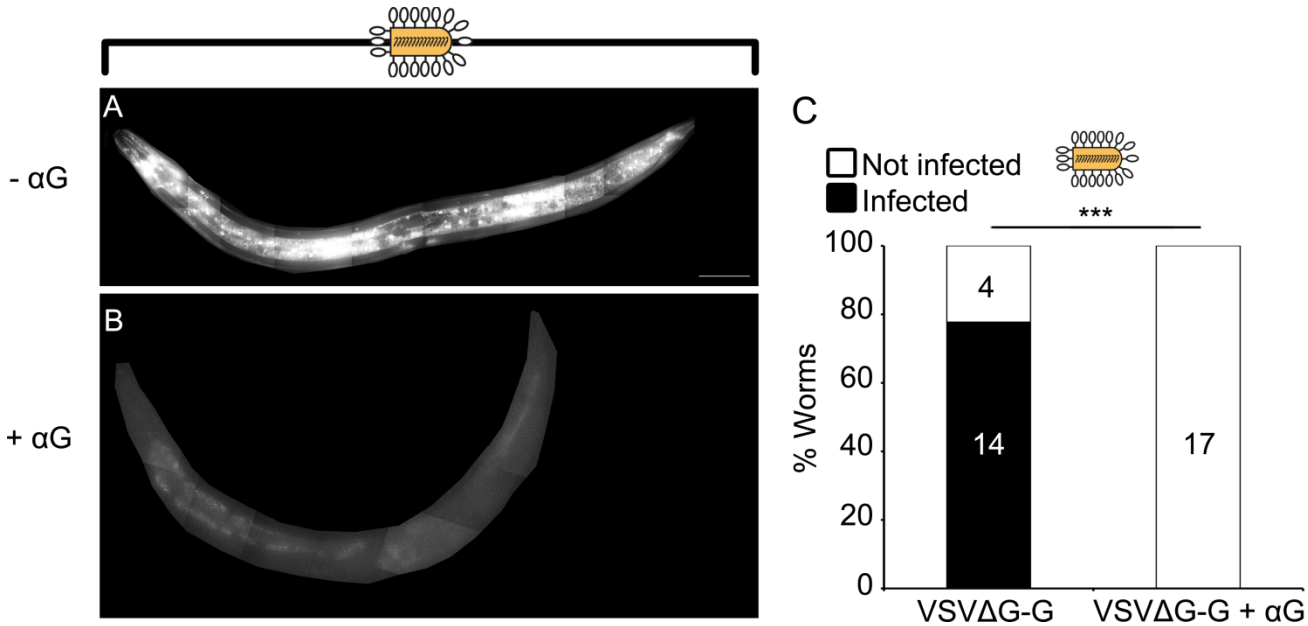


930

931

932 **Figure S4. Anti-VSV-G antibody blocks VSVΔG-G infection in living worms**
933 **(A-B)** SDC microscope Z-stack projections of *drh-1* worms injected with 4700 IU VSVΔG-G
934 that was either not preincubated (-αG), or preincubated with αVSV-G antibody (+αG) and
935 imaged 48 h later. Scale bar, 50 µm.
936 **(C)** Fraction of worms that are infected or not infected with VSVΔG-G or VSVΔG-G +αG.
937 Animals were treated as in (A-B). n=18 and 17 animals for VSVΔG-G and VSVΔG-G+αG
938 respectively. Fisher exact test. p***<0.001.
939

940 **Supplementary tables**

941 **Table S1. Phenotypes of worms with EFF-1 expressed in BWMs**

942

| Genotype | *drh-1(-); hyEx375[myo-3p*::mCherry*, myo-3p*::EFF-1*]* | | |
|---|---|---|---|
| Phenotype/ group | *myo-3p*::mCherry(+) | *myo-3p*::mCherry(-) | P-value |
| wt-like animals | 110 ± 12 (81±3%) | 60 ± 10 (87±6%) | 0.39258 |
| Adult Unc+Dpy | 3 ± 1 (2±1%) | 0 (0%) | 0.05316 |
| Larval-arrested Unc+Dpy | 15 ± 2 (11±1%) | 0 (0%) | 0.00029*** |
| Unhatched eggs | 7 ± 2 (5±1%) | 8 ± 3 (13±6%) | 0.23501 |

943

944 Phenotype count of total progeny from 4 hermaphrodites with extrachromosomal array
945 containing *myo-3p*::EFF-1 and *myo-3p*::mCherry. Data presented as average of the progenies
946 from 4 mothers ±SEM and the percentage out of total relevant group (e.g. *myo-3p*::mCherry(+)
947 or *myo-3p*::mCherry(-)). P-value calculated for certain phenotype fraction (%) in *myo-*
948 *3p::*mCherry(+) vs *myo-3p*::mCherry(-) groups. Two tailed Student's t-test. $p<0.01$***.

949

950 **Table S2. AFF-1/EFF-1 expression in sensory neurons does not induce their infection**
951 **with VSV∆G-AFF-1**
952

| Strain | Genotype | Description | total # of worms | # VSV∆G-AFF-1-infected worms | # worms with GFP(+) cells overlapping with EFF-1/AFF-1 expressing cells |
|---|---|---|---|---|---|
| BP2126 | *drh-1(tm1329); eff-1(hy21); hyEx373 [pmyo-2::GFP, pdes-2::AFF-1(pME4), KS]* | AFF-1 expressed in PVD (Oren-Suissa et al 2017) , in *eff-1(ts)* background | 18 | 6 | 0 |
| BP2131 | *drh-1(tm1329); eff-1(hy21); hyEx374 [pmec-4::EFF-1, pmec-4::dsRed, podr-1::EFF-1,podr-1::dsRed, KS] line1* | EFF-1 expressed in 12 sensory neurons (kind gift from M. Hilliard lab), in *eff-1(ts)* background | 28 | 15 | 0 |
| BP2132 | *drh-1(tm1329); eff-1(hy21); hyEx374 [pmec-4::EFF-1, pmec-4::dsRed, podr-1::EFF-1,podr-1::dsRed, KS] line2* | EFF-1 expressed in 12 sensory neurons, in *eff-1(ts)* background | 22 | 7 | 0 |
| BP2133 | *drh-1(tm1329); eff-1(hy21); hyEx374 [pmec-4::EFF-1, pmec-4::dsRed, podr-1::EFF-1,podr-1::dsRed, KS] line3* | EFF-1 expressed in 12 sensory neurons, in *eff-1(ts)* background | 35 | 13 | 0 |

953
954

955 **Table S3. Reagents, strains, oligos, plasmids and software**

| REAGENT or RESOURCE | SOURCE | IDENTIFIER |
|---|---|---|
| **Antibodies** | | |
| Anti-VSV-G [8G5F11] Antibody | Kerafast | Cat#8G5F-11 |
| **Bacterial and Virus Strains and tissue culture cells** | | |
| Recombinant Vesicular Stomatitis Virus VSVΔG | [68] | VSVΔG |
| *E. coli*: OP50-1 | Caenorhabditis Genetics Center | OP50-1 |
| BHK-21(ATCC) | [69] | BHK-21(ATCC) |
| **Chemicals, Peptides, and Recombinant Proteins** | | |
| FUdR | Sigma | Cat#F0503-1G |
| Tetramisole | Sigma | Cat#L9756-5G |
| Dulbecco's Modified Eagles Medium (DMEM) High glucose, Gibco™ | Thermo Scientific | Cat#41965039 |
| Fugene HD | Promega | Cat#E2311 |
| OptiMEM | Gibco | Cat#31985070 |
| Dulbecco's Phosphate Buffered Saline (DPBS) With Calcium and Magnesium | Biological Industries | Cat#02-020-1A |
| Certified Fetal Bovine Serum (FBS), Heat Inactivated | Biological Industries | Cat#04-121-1A |
| ***C. elegans* strains** | | |
| *drh-1(tm1329) IV* | [7] | *drh-1 (tm1329)* |
| *eff-1(ok1021)II* | [14] | BP347 |
| *drh-1(tm1329) IV; eff-1(ok1021)II* | This paper | BP2122 |
| Strain *eff-1(hy21)II* | [14, 19] | BP75 |
| *drh-1(tm1329) IV; eff-1(hy21)II* | This paper | BP2123 |
| *drh-1(tm1329) IV; aff-1(tm2214)II* | This paper | BP2124 |
| *dzIS53[F49H124p::mCherry] Unknown chromosome* | [70] | EB2110 |
| *drh-1(tm1329) IV; dzIS53[F49H124p::mCherry]* | This paper | BP2121 |
| *trls10 [myo-3p::MB::YFP + myo-2p::YFP + ceh-23::HcRed + unc-25::DsRed + unc-129nsp::CFP]* | Caenorhabditis Genetics Center | RP1 |
| *eff-2 (hy51) II; mcIs46[dlg-1::RFP;unc-119(+)]III* | This paper | BP2104 |
| *drh-1(tm1329) IV ; eff-2(hy51) II* | This paper | BP2125 |
| *drh-1(tm1329)IV; hyEx375 [myo-3p::EFF-1, myo-3p::mCherry, KS bluescript]* | This paper | BP2137 |
| *trls10 [myo-3p::MB::YFP + myo-2p::YFP + ceh-23::HcRed + unc-25::DsRed + unc-129nsp::CFP];hyEx375 [myo-3p::EFF-1, myo-3p::mCherry, KS bluescript]* | This paper | BP2171-3 |
| *drh-1(tm1329) IV; eff-1(hy21) II; hyEx373 [myo-2p::GFP, des-2p::AFF-1, KS bluescript]* | This paper | BP2126 |
| *drh-1(tm1329) IV; eff-1(hy21) II; hyEx374 [mec-4p::EFF-1, pmec-4::dsRed, podr-1::EFF-1, odr-1p::dsRed, KS bluescript]* | This paper | BP2131-3 |
| **Oligonucleotides** | | |
| Primer: *Cloning myo-3p from myo3p::mCherry Plasmid with SalI restriction enzyme: ACGCGTCGAC AGTGATTATAGTCTCTGTTTTC* | This paper | LXH60 |
| Primer: *Cloning myo-3p from myo3p::mCherry Plasmid with NheI restriction enzyme: CTAGCTAGCCATTTCTAGATGGATCTAGTG* | This paper | LXH61 |
| Oligonucleotide: *Conversion oligonucleotide encoding wt pha-1 repair fragment for CRISPR: caaaatacgaatcgaagactcaaaaagagtatgctgtatgattacagatgttcatcaagttattcataaatcattgatag* | This paper | BG123 |
| Primer: *Addition of homology arms to eff-2 around mNeonGreen for CRISPR: ttcctgaagtttcatcaaattcgaagctggcGcgtattttcagaagcATGGTTTCCAAGGGAGAAGAGG* | This paper | BG129 |
| Primer: *Addition of homology arms to eff-2 around mNeonGreen for CRISPR: agattctaatgtgtcagatagtcttgagatcgCtgCgagagaatatactaGACTAGTAGGAAACAGTTATGTTTGG* | This paper | BG130 |
| Primer: *Production of sgRNA plasmid targeting eff-2 at locus AGAAGCAGAATAAACTGGGGAGG for CRISPR: AGAAGCAGAATAAACTGGGGGTTTTAGAGCTAGAAATAGC* | This paper | BG84 |
| Primer: *Production of sgRNA plasmid targeting eff-2 at locus AGAAGCAGAATAAACTGGGGAGG for CRISPR: CCCCAGTTTATTCTGCTTCTAAACATTTAGATTTGCAATTC* | This paper | BG85 |

| | | |
|---|---|---|
| **Recombinant DNA** | | |
| Plasmid pCAGGS-Gind: *pCAGGS::VSV-G Indiana* | [68] | pCAGGS-Gind |
| Plasmid pOA20: *pCAGGS::aff-1::FLAG* | [6] | pOA20 |
| Plasmid pKSI-1: pBluescript empty vector | [71] | Addgene plasmid #51725 |
| Plasmid pXH20: *myo-3p::EFF-1* | This paper | pXH20 |
| Plasmid pME1: *hsp16.2::EFF-1* | [19] | pME1 |
| Plasmid pCFJ104: *myo-3p::mCherry* | [72] | Addgene plasmid #19328 |
| Plasmid pBG115: *CeU6p::eff-2_sgRNA for CRISPR* | This paper | pBG115 |
| Plasmid pDD162: *eft-3p::Cas9 + Empty sgRNA for CRISPR* | [73] | Addgene plasmid #47549 |
| Plasmid pJW1285: *eft-3p::Cas-9-SV40 NLSNLS::tbb-2 3'UTR + CeU6p::pha-1_sgRNA for CRISPR* | [74] | Addgene plasmid #61252 |
| Plasmid pNG1: *dlg-1p::Lifeact::mNeonGreen* | Kind gift of A. Hajnal | pNG1 |
| PCR amplicon: *mNeonGreen flanked by homology arms to the eff-2 gene for CRISPR* | This paper | N/A |
| Plasmid : *odr-1p::dsRed* | [24] | odr-1p::dsRed |
| Plasmid: *odr-1p::EFF-1* | [24] | odr-1p::EFF-1 |
| Plasmid: *mec-4p::EFF-1* | [24] | mec-4p::EFF-1 |
| Plasmid: *mec-4p::mCherry* | [24] | pmec-4::mCherry |
| **Software** | | |
| Fiji | NIH image | |
| GraphPad Prism 8 | GraphPad Software, Inc. | |
| Adobe Photoshop CS5 and CS6 | Adobe | |
| MetaMorph 7.8.1.0 | Molecular Devices | https://www.moleculardevices |
| Micro-Manager | [75] | https://micro-manager.org |

956

957 **Data for movies**

**Movie S1. EFF-1 ectopic expression in BWMs results in Uncoordinated and Dumpy (Unc+Dpy) phenotypes**

Mixed population of worms with extrachromosomal *pmyo-3::mCherry* and *pmyo-3::EFF-1.* White arrowhead point to mCherry(+) worm that is Unc+Dpy. White arrow point to mCherry(+) worm that is wt-like. Yellow arrowhead points to a wt-like mCherry(-) worm, which left the frame within seconds. Elapsed time (seconds) indicated in top left corner.

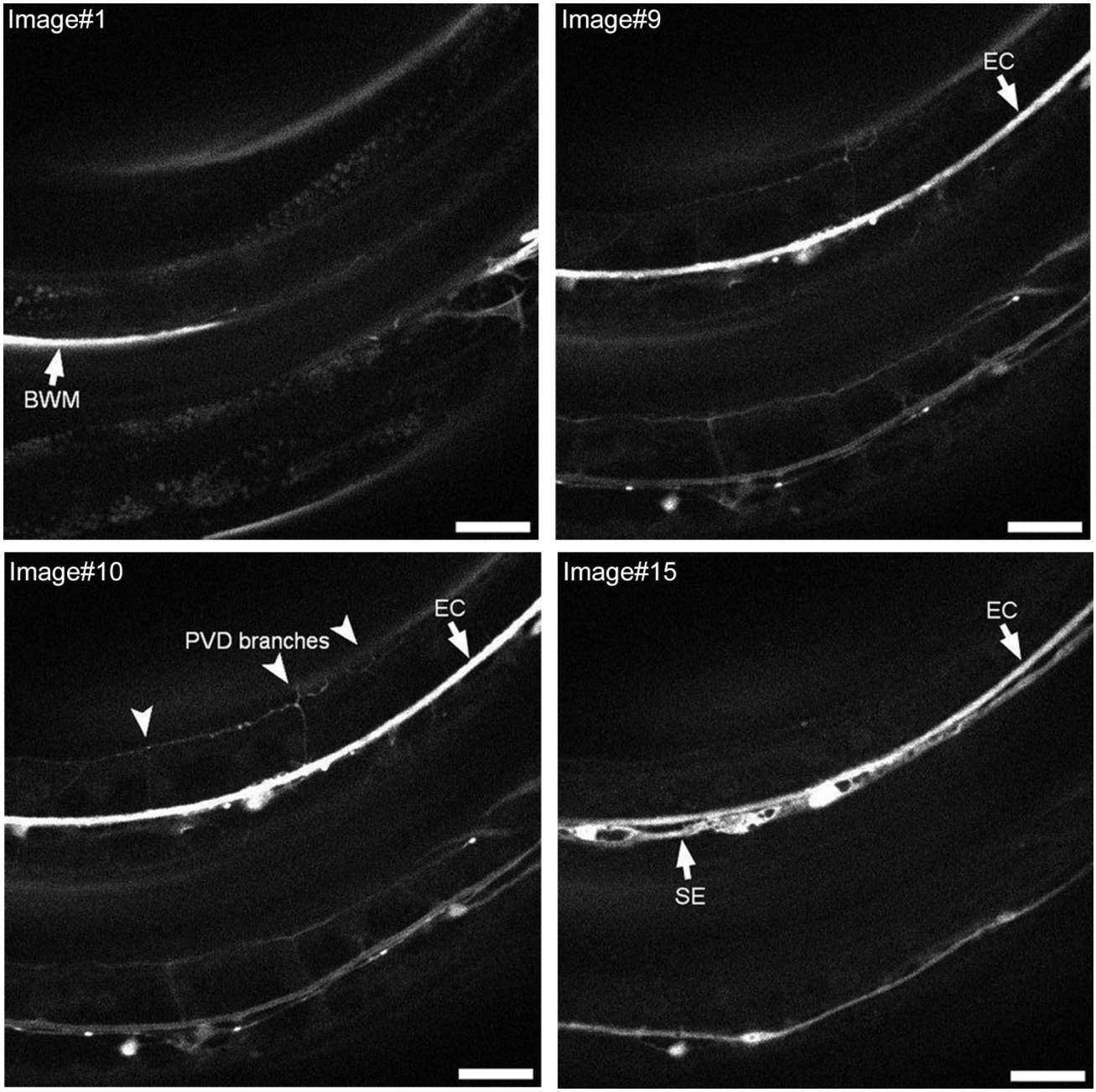


977

978

979 **Movie S2. VSVΔG-G infects PVD neuron**

980 SDC microscope Z-stack of young adult worm injected with $10^6$ IU VSVΔG-G and imaged 48h
981 later. Arrowheads, infected PVD's candelabra/menorahs arborized branches. Arrows, infected
982 cell. BWM-Body Wall Muscle, EC-Excretory Cell, SE-Seam cell syncytium. Scale bars, 25 μm.
983 Note that there is a second worm (bottom, not indicated in images), also showing infected
984 PVD branches, EC, SE and a muscle cell.